Assessment of Surface-Heating Problems in Laser-Fusion Reactors

S.I. Abdel-Khalik and T.O. Hunter

February 1977

UWFDM-197

FUSION TECHNOLOGY INSTITUTE

UNIVERSITY OF WISCONSIN

MADISON WISCONSIN

Assessment of Surface-Heating Problems in Laser-Fusion Reactors

S.I. Abdel-Khalik and T.O. Hunter

Fusion Technology Institute
University of Wisconsin
1500 Engineering Drive
Madison, WI 53706

http://fti.neep.wisc.edu

February 1977

UWFDM-197

"LEGAL NOTICE"

"This work was prepared by the University of Wisconsin as an account of work sponsored by the Electric Power Research Institute, Inc. ("EPRI"). Neither EPRI, members of EPRI, the University of Wisconsin, nor any person acting on behalf of either:

"a. Makes any warranty or representation, express or implied, with respect to the accuracy, completeness, or usefulness of the information contained in this report, or that the use of any information, apparatus, method, or process disclosed in this report may not infringe privately owned rights; or

"b. Assumes any liabilities with respect to the use of, or for damages resulting from the use of, any information, apparatus, method or process disclosed in this report."

Assessment of Surface-Heating Problems in Laser-Fusion Reactors

by

S. I. Abdel-Khalik and T. O. Hunter*

Nuclear Engineering Department and Fusion Technology Program

University of Wisconsin - Madison, Wisconsin 53706 USA

ABSTRACT

The surface-heating problems associated with the pulsed photon and ion irradiations of the first walls and liners of inertially-confined fusion reactor cavities are investigated. Analytical models for predicting the thermal response of these surfaces as a function of the different design and operational parameters of the system and the nature of the incident irradiations are developed. The effectiveness of residual gas as a means for protecting the wall from the ions and soft X-rays is assessed.

Generalized charts are given for predicting the surface temperature rise produced by the reflected laser light and X-rays emanating from the microexplosion. Similar results are given for alpha particles (50-500 kev) with carbon and tantalum as liner materials. The resulting temperature histories are used to estimate the surface evaporation rates.

---

*Member Technical Staff, Sandia Laboratories, Albuquerque, N.M. 87115.
Work partially supported by U.S.E.R.D.A.

NOMENCLATURE

A	Parameter defined after Eqs. (3)
b	Nondimensional absorption coefficient
c	Specific heat
E	Particle energy
E_1	Incident particle energy
$f(t)$, $F(\theta)$	On/off control function in Fig. 1
g, g_o	Volumetric heat generation rates
G	Green's function
k	Thermal conductivity
L	Wall thickness
M	Molecular weight
N	Number of complete pulses prior to t
$\dot{n}$	Evaporation rate
p	Vapor pressure
q, q_o	Surface heat flux
Q	Nondimensional heat generation function
$S(E)$	Particle energy spectrum
t	Time
T	Temperature
T_o	Back surface temperature
u, u_a, u_b	Nondimensional temperature
x	Position coordinate
x_m	Particle range

Greek Symbols

α	Thermal diffusivity
$\delta\omega$	Time after end of previous pulse
ε_p	Photon energy
ζ_i	Parameter defined in Eq. (6)
θ	Nondimensional time
κ	Nondimensional pulse width
μ	Absorption coefficient
ξ	Nondimensional position coordinate
ρ	Density
τ, τ^*	Reference time for exponentially-decaying surface heat flux
ω	Time between pulses
Ω	Nondimensional time between pulses

INTRODUCTION

The energy release from the exploding pellets of inertially-confined fusion reactors consists of energetic neutrons, photons, and charged particles which eventually dissipate their kinetic energies in the walls surrounding the reactor cavity. For dry-wall type cavities, the surface-heating and ablation of the first wall (or its protective liner) by the X-rays and charged particles emanating from the pellet and by the reflected laser light may be the limiting factors in determining the necessary cavity size to contain the microexplosion. These photons and charged particles have a relatively short range, and as a result, the surface temperature of the wall may rise sharply after each pulse.

Calculations of the implosion of bare D-T pellets indicate that approximately 1% of the energy yield is in the form of X-rays.[1-5] Structured pellets may produce higher X-ray fractions with softer spectra. This tends to exacerbate the surface-heating problem since softer X-rays have a shorter range. The majority of these X-rays are produced during the thermonuclear burn which lasts about 10 ps, however, for structured pellets, the X and gamma radiation occurs over a longer time interval.[1,4]

A significant portion (20-25%) of the energy yield from the microexplosion is released in the form of energetic charged particles. For some pellet designs, the alpha particles escaping from the pellet may carry as much as one-third of that energy; the remainder is associated with the pellet debris. These include the unburned deuterons, tritons and trapped alphas, as well as any non-hydrogenic pellet constituents. The arrival times at the first wall of free-streaming charged particles and of the debris plasma depend on chamber geometry and dimensions, and on the kinetic energy and spectra of the particles. These times are also affected by the presence of a magnetic field or significant amounts of residual gas in the chamber. Knowledge of the spatial energy deposition as a function of particle energy, and the arrival time of each particle is necessary for evaluating the thermal response of the wall.

A significant fraction of the incident laser light can be reflected from the DT plasma surrounding the pellet before reaching the critical plasma density.[2] This reflection may persist for time periods of the order of 100 ps. Similar to the X-rays and charged particles, the reflected laser light will result in rapid surface heating in the first wall because of its short range.

It is the purpose of this investigation to develop general models for predicting the thermal response of candidate materials for first walls and liners to these pulsed photon and ion irradiations. The effectiveness of residual gas as a means for protecting the wall from the ions and soft X-rays is assessed. The presence of a significant amount of gas in the reactor cavity will affect the temperature response of the first wall inasmuch as it modifies the photon spectra and slows down (or stops) the ions.

THEORETICAL ANALYSIS

Response to Photon Irradiation With No Residual Gas

Reactor cavities are either spherical or cylindrical with diameters considerably larger than the first wall or liner thickness. Hence, the wall (or liner) can be represented by a slab as shown in Fig. (1-a). If the pressure inside the cavity is sufficiently low, the photons will not be attenuated and will deposit their energies directly in the liner. Under these conditions, radiative and convective heat flux at the liner's inner surface can be ignored. The outside surface can be assumed to remain at a constant temperature T_o throughout the transient. This condition can be physically realized if the thermal time constant of the liner is considerably larger than the time between

pulses. Under these conditions, the pulsating volumetric heating loads are rectified and a constant heat flux is radiated or convected from the back surface. The initial temperature distribution in the liner is assumed to be uniform and equal to T_0. This assumption should not affect the sustained transient solution in which we are interested.

For a pulsating flux of monoenergetic photons, the volumetric heat generation rate, g, can be represented by:

$$g(x,t) = (g_0\, \bar{e}^{\mu x})\, f(t) \tag{1}$$

where g_0 is the volumetric heat generation rate at the surface, μ is the absorption coefficient, and f(t) is the on/off control function shown in Fig. (1-b). The time between pulses and the pulse width are assumed to be constant and equal to ω and $\kappa\omega$ respectively. The surface heat generation rate g_0 is related to the incident flux ϕ_0, absorption coefficient μ, and photon energy ε_p by the relation: $g_0 = \phi_0 \mu\, \varepsilon_p$. The incident flux ϕ_0 is assumed to remain constant during the "on" period so that g_0 is not a function of time. It is a straightforward matter, however, to extend the analysis to include any temporal flux variations.

We introduce the nondimensional variables:

$$\left.\begin{aligned} u &\equiv (T - T_0) \,/\, [(g_0/\mu)\, \kappa\omega/\rho cL] \\ \xi &\equiv x/L \\ \theta &\equiv \alpha t/L^2 \end{aligned}\right\}. \tag{2}$$

In Eq. (2), the nondimensional temperature $u(\xi,\theta)$ is the ratio between the actual temperature rise and that obtained if the incident photons' energy were to be

deposited uniformly and adiabatically. In terms of these nondimensional variables, the heat conduction equation, boundary conditions, and initial condition for the above stated problem are:

$$\frac{\partial^2 u}{\partial \xi^2} + Q(\xi)\, F(\theta) = \frac{\partial u}{\partial \theta} \tag{3a}$$

$$\left.\begin{aligned} \frac{\partial u}{\partial \xi}(o,\theta) &= o \\ u(1,\theta) &= o \end{aligned}\right\} \tag{3b}$$

$$u(\xi,o) = o\ . \tag{3c}$$

The nondimensional heat generation function $Q(\xi)$ is given by: $Q(\xi) = A\, e^{-b\xi}$; $o \leq \xi \leq 1$, where $A \equiv b/\kappa\Omega$, $b \equiv \mu L$, and $\Omega \equiv \alpha\omega/L^2$. The on/off function $F(\theta)$ is shown in Fig. (1-b).

The sustained transient solution, $\tilde{u}(\xi,\theta)$, for the above stated problem is given by:

$$\tilde{u}(\xi,\theta) = 2 \sum_{n=1}^{\infty} \cos\left[\left(\frac{2n-1}{2}\right)\pi\xi\right] \left\{\frac{b^2}{b^2+\left(\frac{2n-1}{2}\pi\right)^2}\right\}$$

$$\left\{1 + e^{-b}\left(\frac{2n-1}{2b}\pi\right)\sin\left(\frac{2n-1}{2}\pi\right)\right\} \left\{\frac{\exp\left[-\left(\frac{2n-1}{2}\pi\right)^2 \delta\Omega\right]}{\left(\frac{2n-1}{2}\pi\right)^2 \kappa\Omega}\right\}$$

$$\left\{\left[\exp\left[\left(\frac{2n-1}{2}\pi\right)^2 \delta\Omega\right]-1\right] + \frac{\exp\left[\left(\frac{2n-1}{2}\pi\right)^2 \kappa\Omega\right]-1}{\exp\left[\left(\frac{2n-1}{2}\pi\right)^2 \Omega\right]-1}\right\}$$

$$(o \leq \delta \leq \kappa) \tag{4}$$

and,

$$\tilde{u}(\xi,\theta) = 2 \sum_{n=1}^{\infty} \cos\left[\left(\frac{2n-1}{2}\right)\pi\xi\right] \left\{\frac{b^2}{b^2+\left(\frac{2n-1}{2}\pi\right)^2}\right\} \left\{1 + e^{-b}\left(\frac{2n-1}{2b}\pi\right) \sin\left(\frac{2n-1}{2}\pi\right)\right\} \left\{\frac{\exp\left[-\left(\frac{2n-1}{2}\pi\right)^2 \delta\Omega\right]}{\left(\frac{2n-1}{2}\pi\right)^2 \kappa\Omega}\right\} \left\{\frac{\exp\left[\left(\frac{2n-1}{2}\pi\right)^2 \kappa\Omega\right]-1}{1-\exp-\left[\left(\frac{2n-1}{2}\pi\right)^2 \Omega\right]}\right\}$$

$$(\kappa \leq \delta \leq 1) \ . \qquad (5)$$

In Eqs. (4) and (5), the fraction δ is defined by: $\theta = (N + \delta)\Omega$, where N is an integer much larger than unity.

Equations (4) and (5) can be used to determine the nondimensional transient temperature distribution in the liner resulting from the pulsating exponential heat deposition given by Eq. (1). After a large number of pulses, the surface temperature will vary in a cyclic manner between a maximum value, u_{max}, at

$\delta = \kappa$ and a minimum value, u_{min}, at $\delta = 1$. These temperature extremes are of particular significance when estimating the stress levels produced in the liner. These are necessary for determining whether spallation will take place.

For small values of Ω, i.e. when the time constant of the liner is considerably larger than the time between pulses, u_{min} will depend only on the nondimensional absorption coefficient b, while u_{max} will depend on both b and the nondimensional pulse width κ. Plots of u_{min} and u_{max} as functions of b and κ for $\Omega = 0.01$ are shown in Fig. (2). These results are quite general inasmuch as they can be used for arbitrary geometry, material, absorption coefficient (i.e. photon energy), repetition rate, wall loading, and pulse width. In the following, we show how these results can be directly used to determine the surface temperature rise produced by the reflected laser light for different lasers and pellet "reflectivities." The results shown in Fig. (2) are also used, along with superposition techniques, to determine the surface temperature rise produced by the X-rays emanating from the microexplosion.

Temperature Rise Produced by the Reflected Laser Light

For low-energy photons, the attenuation coefficient μ in the exponential heat deposition curve of Eq. (1) may be estimated by considering the attenuation of electromagnetic radiation in a homogeneous, isotropic, conducting medium with zero surface reflectivity. The result is $\mu = 8\pi/\lambda$ where λ is the wavelength.[6] Therefore, the results shown in Fig. (2) can be readily used to determine the surface temperature rise produced by the reflected laser light for a given system geometry and operating conditions.

A 6.5 mm thick graphite liner in a 12 m diameter cavity is considered. For a 1 MJ laser with a repetition rate of 20 sec^{-1} and a pellet "reflectivity"

of 15%, the surface temperature rise is plotted in Fig. (3) for different laser wavelength and pulse width. These results can be easily used for other conditions since $\Delta T_{surface}$ is linearly proportional to the incident flux. It should be emphasized that the results shown in Fig. (3) do not account for any evaporation which may take place at the liner surface. Figure (3) is quite valuable inasmuch as it allows us to estimate the maximum tolerable pellet reflectivity corresponding to the onset of liner sublimation or spallation.

Temperature Rise Produced by the X-rays

It is important to be able to determine the thermal response of the liner when subjected to a pulsating photon source with an arbitrary spectrum. This task can be readily accomplished by extending the solution for monoenergetic photons by means of superposition techniques. The X-ray spectra produced by the microexplosions are approximated by black-body radiations in the range of 0.1-2.0 keV. This range is sufficiently wide to cover pellet designs of interest.

The spectrum is divided into M bands with average photon energies ε_i, $i = 1, 2, \ldots, M$. Let ζ_i be the fraction of the incident energy within band i so that:

$$\sum_{i=1}^{M} \zeta_i = 1 \ . \qquad (6)$$

The surface flux from the pulsating black-body source is given the symbol S so that the incident energy within a single pulse per unit surface area is equal to $S\kappa\omega$. We assume that the incident photons within the different bands will result in exponential heat deposition curves with absorption

coefficients μ_i, i = 1, 2, . . ., M, so that the corresponding net heat generation rate g(x,t) can be represented by:

$$g(x,t) = f(t)\, S \sum_{i=1}^{M} \zeta_i\, \mu_i\, e^{-\mu_i x} \quad . \tag{7}$$

The linearity of Eqs. (3a, b) allows the superposition of monoenergetic results so that:

$$u(\xi,\theta) = \sum_{i=1}^{M} \zeta_i\, u_i(\xi,\theta) \tag{8}$$

where $u_i(\xi,\theta)$ is the solution to Eqs. (3a-c) given by Eqs. (4) and (5) with b equal to b_i.

For graphite, the absorption coefficients are curve fitted for five ranges of photon energies: (0.01-0.284 kev), (0.284-0.80 kev), (0.80-4.00 kev), (4.0-20.0 kev), and (20.0-100.0 kev) using relations of the form:[7]

$$(\mu/\rho)\ (cm^2/g) = \sum_{j=1}^{4} a_j/\varepsilon_p^j \quad ,$$

where ε_p is the photon energy in kev. The constants a_j, j = 1 - 4 for the five ranges of photon energies are given in reference [7].

A 6.5 mm thick graphite liner in a 12 m diameter cavity is considered. For a pellet yield of 150 MJ, a repetition rate of 20 sec^{-1}, and an X-ray fraction of 1%, the periodic surface temperature rise is shown in Fig. (4) for different black-body temperatures and pulse duractions. Obviously, softer spectra produce higher surface temperature jumps because of their shorter range. The case κ = 0 corresponds to instantaneous deposition of the X-ray energy into the liner. Similar results for niobium are shown in Fig. (5).

Again, it should be emphasized that the results shown in Figs. (4) and (5) do not account for any evaporation which may take place at the liner surface. However, these results should help in determining the conditions corresponding to the onset of liner sublimation or spallation.

Thermal Response to Pulsed Ion Sources With No Residual Gas

The thermal response of the wall (or liner) to ion pulses can be determined upon knowledge of the spatial energy deposition as a function of particle energy and arrival time of each particle. A model has been developed whereby a given spectrum of particles is initiated at the cavity center and each particle is allowed to propagate uncollided to the point of impact. The resulting particle arrival density is combined with their slowing-down characteristics to yield the spatial and temporal distribution of energy deposition. This, in turn, is used to determine the thermal response of the wall.

The particle energy loss is usually calculated as a function of its local kinetic energy. For electronic losses described by modified Linhard slowing down model,[8] the rate of energy loss is given by

$$\frac{dE}{dx} = - C \left(\frac{E}{E_o}\right)^{1/2} . \qquad (9)$$

For a particle with incident energy E_1, Eq. (9) can be transformed from spectral to spatial dependence as:

$$\frac{dE}{dx}(x) = \frac{xC^2}{2E_o} - C\left(\frac{E_1}{E_o}\right)^{1/2} . \qquad (10)$$

The particle range, $x_m(E_1)$, is given by:

$$x_m(E_1) = \frac{2(E_o E_1)^{1/2}}{C} \quad . \tag{11}$$

The particles from a pulsed source will arrive at a given location with an arrival density function f(t) given by:

$$\int_t f(t)\, dt = -\int_E S(E)\, dE \quad . \tag{12}$$

Here, the integral is equal to the total number of incident particles per unit surface area, and S(E) is the particle energy spectrum at x = o. If the kinetic energy of the particles is primarily directed along the propagation axis (i.e. small thermal component), the arrival density would be given by:

$$f(t) = 2S(E)\, E^{3/2}/B \tag{13}$$

where, $B = 2.284 \times 10^{-6}\, RA^{1/2}$. Here, R is the distance travelled by the particles (i.e. cavity radius) in meters and A is the particle mass in amu.

The volumetric heating rate is related to the arrival density function by: $g(x,t) = f(t)\, \frac{dE}{dx}(x)$. Therefore,

$$\left.\begin{aligned} g(x,t) &= f(t)\, \left[\frac{A_1}{t} - A_2\, x\right]; \quad x < \frac{2BE^{1/2}}{Ct} \\ &= o \qquad\qquad\qquad\quad ; \quad x > \frac{2BE_o^{1/2}}{Ct} \end{aligned}\right\} \tag{14}$$

where $A_1 \equiv (CB/E_o^{1/2})$, $A_2 \equiv C^2/2E_o$, and $(B/\sqrt{E}_{max} < t < B/\sqrt{E}_{min})$. Here, E_{min} and E_{max} are the limits of the spectrum.

For a semi-infinite solid with an insulated boundary at x = o, and volumetric heat source g(x,t), the transient temperature distribution is given by:[9]

$$T(x,t) = \iint_{tx} \frac{g(x',t')}{\rho c}\, G(x,t,x',t')\, dx'\, dt'$$

where G is Green's function given by:

$$G(x,t,x',t') = \frac{1}{2\sqrt{\pi\alpha(t-t')}} \left\{ \exp\left[-(x - x')^2/4\alpha\,(t - t')\right] + \exp\left[-(x + x')^2/4\alpha\,(t - t')\right] \right\} .$$

For the volumetric heat source given by Eq. (14), the above equation yields:

$$T(x,t) = \frac{1}{\rho c} \int_{t_{min}}^{t_{max}} f(t') \left\{ Q_1(t',t,x) + Q_2(t',t,x) + Q_3\,(t',t,x) \right\} dt' \qquad (15)$$

where

$$\left.\begin{aligned} Q_1(t',t,x) &= \frac{A_1}{2t'} \left[\operatorname{erf}(F_1) + \operatorname{erf}(F_2)\right] , \\ Q_2(t',t,x) &= \frac{A_2 x}{2} \left[\operatorname{erf}(F_2) - \operatorname{erf}(F_1) - 2\operatorname{erf}(F_o)\right] , \\ Q_3(t',t,x) &= A_2 \sqrt{\frac{\alpha(t-t')}{\pi}} \left[\bar{e}^{F_2^2} + \bar{e}^{F_1^2} - 2\bar{e}^{F_o^2}\right] , \\ F_o &\equiv x/2\sqrt{\alpha(t-t')} , \\ F_1 &= (x_m - x)/2\sqrt{2\alpha(t-t')} , \\ F_2 &= (x_m + x)/2\sqrt{2\alpha(t-t')} , \end{aligned}\right\}$$

and

$$\left.\begin{aligned} x_m &= 2BE_o^{1/2}/Ct' . \end{aligned}\right\} \qquad (16)$$

The above analysis has been carried out for intermediate energy ions characteristic of pellet debris which can be described by the modified Linhard slowing down model [8] (Eq. 9). For heavier ions, the inclusion of nuclear stopping will alter the deposition profiles to be more spatially uniform. Incorporation of this effect yields a result similar to Eq. (15). In all cases, the time integral is performed numerically so that arbitrary spectra can be accommodated. The use of the semi-infinite solid model to predict the temperature response of the liner to ion irradiation should be quite accurate since the ions' range is extremely short compared to practical wall thicknesses.

Results are shown for 200 kev Maxwellian spectra in a 12 m diameter cavity. Figure 6 shows the arrival flux density of He and Si particles as a function of time. Figure 7 shows the time-dependent energy deposition rate at various distances from the front surface for helium in carbon. The corresponding temperature response is shown in Fig. 8. Similar results for silicon ions in carbon and helium ions in tantalum are shown in Figs. 9 and 10 respectively.

The results shown in Figs. 8-10 have been normalized to an ion wall loading of 1 J/cm^2 per pulse. Ion fluxes for conceptual laser fusion reactors can be much higher than 1 J/cm^2 per pulse.[10] The resulting temperatures would be too high for wall survival and protective measures must be employed. In the following, we shall investigate the effectiveness of residual gas as a means for protecting the wall from the ions and soft X-rays emanating from the microexplosion.

Effect of Residual Chamber Gas

The gas pressure inside the reactor cavity has to be sufficiently low to allow laser propagation and focusing onto the pellet. Neon has the highest laser-induced gas breakdown threshold followed closely by helium[11]. Thus, for a given laser intensity, neon can be maintained at the highest pressure and still transmit the laser beams. For example, for 1 μm light with an on-target intensity of 10^{16} W/cm^2, the reactor cavity can be filled with neon at a pressure of about 1 torr. At such pressures, the gas can significantly modify the X-ray spectra incident on the wall by absorbing the low-energy photons (Fig. 11). These photons would have produced high surface temperature excursions because of their short range. Figure 12 shows how a black body spectrum initiated at the center of a neon-filled, 12 m diameter cavity is modified. The wall will, therefore, be subjected to harder X-ray spectra than those produced by the microexplosion. These produce considerably lower surface temperatures because of their longer range.

Typical results showing the surface temperature rise produced by the modified X-ray spectra are shown in Fig. 13. These results pertain to a 6.5 mm thick graphite liner in a neon-filled, 12 m diameter cavity. The results are plotted against the black body temperature characterizing the original spectrum produced by the microexplosion. Figure 14 shows the surface temperature rise for different gas pressures and black body temperatures with zero pulse width. These results show that gas protection can be quite effective especially if the X-rays produced by the microexplosion are soft as may be the case with structured pellets[1,4].

In addition to absorbing the soft X-rays, the gas can stop the ions produced by the microexplosion. If the wall radius exceeds the mean ion

range by approximately a factor of 2, all the ions' kinetic energy will be deposited in the chamber gas. The neon pressure corresponding to a mean range of 6 m is shown in Fig. 15 for a variety of ions. These data are based on ion range calculations using Lindhard theory in the EDEPI code [12]. These results indicate that most of the non-hydrogenic pellet constituents can be stopped in the gas at sufficiently low pressures.

The energy deposited in the gas by the X-rays and ions will be removed by radiation to the chamber walls and gas ejection through the vacuum system. (A steady stream of cold gas is allowed into the system). Unless the energy is radiated to the wall over a sufficiently long period, excessive surface heating and ablation would result. The temporal distribution of the radiant heat flux depends on the radiation transport through the gas, as well as system characteristics. Here we consider the two limiting cases shown in Figs. 16a and b. For case a, the radiant heat flux during each pulse is assumed to remain constant and equal to q_o over a period $\kappa\omega$, where ω is the time between pulses. For case b, the surface heat flux during each pulse is assumed to decay exponentially so that for the (N+1) pulse: $q = q_o \exp[-(t-N\omega)/\tau]$; $N\omega \leq t \leq (N+1)\omega$, where τ is a reference time.

The thermal response of a finite slab of thickness L subjected to a sequence of these heat flux pulses can be readily obtained by either superposition or variation of parameters techniques [9]. The back surface of the slab (x=L) is assumed to remain at a constant temperature T_o. For case a, the sustained transient solution $\tilde{u}_a(\xi,\theta)$ is given by:

Typical results showing the surface temperature rise in a graphite wall subjected to a train of heat flux pulses of types a and b are shown in Figs. (17) and (18) respectively. These results do not account for any evaporation which may take place at the surface. It is obvious that the surface temperature rise, and hence the maximum surface temperature, will decrease as the pulse width is increased. For the case shown, in order to prevent excessive evaporation and spallation of the wall, the energy deposited in the gas has to be radiated over a period $\geq \sim 1$ ms. This, in turn, can be used to determine the necessary amount of gas in the chamber to provide such a long cool-down period.

Surface Evaporation Rate

The evaporation rate from a surface at temperature T can be estimated from the equilibrium vapor pressure p of the solid material above the surface. The evaporation rate $\dot{n}(T)$ is given by[13]:

$$\dot{n}(T) = \frac{3.5 \times 10^{22}}{\sqrt{M}} \frac{p}{\sqrt{T}} \left(\frac{\text{atoms}}{\text{cm}^2 \text{ sec}}\right) \tag{20}$$

where M is the molecular weight, p is in torr, and T is in °K. Vapor pressure data for several first wall materials are given in reference [13]. Upon knowledge of the surface temperature history and the corresponding vapor pressure, one can determine the evaporation rate as a function of time. Typical results for a graphite wall subjected to black body radiation with no gas protection are shown in Fig. 19. These can be integrated to determine the amount of material ablated per pulse (Fig. 20). These results indicate that unless some means for wall protection is provided, excessive evaporation can take place.

CONCLUSIONS

General models for evaluating the thermal response of the first wall (or its protective liner) produced by the X-rays and charged particles emanating from the pellet and by the reflected laser light have been developed. These models are quite general inasmuch as they can be used for arbitrary geometry, wall material, spectra, repetition rate, wall loading, and pulse width. The results are presented in a parametric fashion so that the maximum tolerable limits, e.g. pellet "reflectivity", X-ray fraction, or ion wall loading, corresponding to the onset of liner spallation or sublimation can be determined.

The effect of residual chamber gas on X-ray spectra and ion-stopping has been examined. Gases such as neon at $\sim$ 1 torr are observed to significantly reduce the direct X-ray heating and to stop the energetic ions. The reradiation of this energy can however produce large temperature excursions unless the energy is radiated over a sufficiently long period ($\sim$ 1 ms).

Evaporation rates from the temperature histories of the above models indicate that materials such as carbon can suffer a significant amount of material loss unless some protection measures are provided.

ACKNOWLEDGEMENT

This work has been supported by the Electric Power Research Institute under contract RP 237-3. Financial support for TOH has been provided by Sandia Laboratories.

REFERENCES

1. G. A. Moses and G. R. Magelssen, "PHD-IV, A Laser-Plasma Simulation Code", Trans. Am. Nucl. Soc. 27 (1977) 39.

2. A. J. Glass and K. L. Cummings (Eds.), "Laser Program Annual Report", Lawrence Livermore Laboratory (1975).

3. J. M. Williams et al., "Engineering Design for Laser Controlled Thermonuclear Reactors", Proc. 5th Symposium on Engineering Problems of Fusion Research, Princeton, NJ (1973).

4. T. G. Frank et al., "Heat Transfer Problems Associated with Laser Fusion", Proc. 6th National Heat Transfer Conference, St. Louis (1976).

5. J. Hovingh et al., "The Preliminary Design of a Suppressed Ablation Laser-Induced Fusion Reactor", Proc. 1st Topical Meeting on the Technology of Controlled Nuclear Fusion, CONF-740402-P1, San Diego (1974).

6. J. Hovingh, "First Wall Studies of a Laser-Fusion Hybrid Reactor Design", Proc. 2nd Topical Meeting on the Technology of Controlled Nuclear Fusion, Richland, Washington (1976).

7. F. Biggs and R. Lighthill, "Analytical Approximations for X-ray Cross-Sections II", SC-RR-71-0507, Sandia Laboratories (1971).

8. J. Lindhard, M. Scharff and H. E. Schiott, Mat. Fys. Medd. Dan. Vid. Selsk., 33, 14 (1963).

9. H. S. Carslaw and J. C. Jaeger, Conduction of Heat in Solids, Second Edition, Oxford University Press (1959).

10. R. W. Conn, S. I. Abdel-Khalik, and G. A. Moses, "SOLASE, A Laser Fusion Reactor Study", Trans. Am. Nucl. Soc. 27 (1977) 36.

11. R. G. Tomlinson, E. K. Damon, and H. T. Buscher, "The Breakdown of Noble and Atmospheric Gases by Ruby and Neodymium Laser Pulses", Physics of Quantum Electronics, Kelley, Lax, and Tannenwald (Eds.), p. 520, McGraw Hill, New York (1966).

12. I. Manning and G. P. Mueller, "Depth Distribution of Energy Deposition by Ion Bombardment", Computer Physics Communication, 6 (1973).

13. R. Behrish, "First Wall Erosion in Fusion Reactors", Nuclear Fusion, 12, 695 (1972).

Figure Captions

Figure 1: Schematic representation of the liner and time dependence of the volumetric heat generation function f(t).

Figure 2: Variation of the nondimensional surface temperature with pulse width and nondimensional absorption coefficient.

Figure 3: Variation of the surface temperature rise produced by the reflected laser light with wavelength and pulse duration (6.5 mm thick graphite liner).

Figure 4: Variation of the surface temperature rise produced by the X-rays with black body temperature and pulse duration (6.5 mm thick graphite liner).

Figure 5: Results similar to Fig. 4 for a niobium wall.

Figure 6: Arrival flux density of He and Si particles in a 12 m diameter cavity.

Figure 7: Variation of the energy deposition rate, g(x,t), with time and location for helium ions incident on a carbon wall.

Figure 8: Temperature response of a carbon wall bombarded by helium ions. (Ion wall loading is normalized to 1 J/cm^2 per pulse).

Figure 9: Results similar to Figure 8 for silicon ions in carbon.

Figure 10: Results similar to Figure 8 for helium ions in tantalum.

Figure 11: Attenuation of X-rays in neon for different spectra and gas pressures.

Figure 12: Modified spectra as a function of gas pressure for 0.5 keV black body radiation (the discontinuities result from K-edge absorption in neon).

Figure 13: Variation of the surface temperature rise produced by the modified X-ray spectra for a gas pressure of 1 torr (6.5 mm thick graphite liner; the black body temperatures refer to the original spectrum).

Figure 14: Variation of the surface temperature rise produced by the modified X-ray spectra with gas pressure for a zero pulse width (6.5 mm thick graphite liner).

Figure 15: Neon pressures corresponding to a mean range of 6 m for a variety of ions.

Figure 16: Schematic diagrams showing the two surface heat flux distributions considered in this investigation.

Figure 17: Variation of temperature rise produced in a graphite wall by a train of square heat flux pulses with pulse width. (T_{max} and $\Delta T_{surface}$ are the maximum surface temperature and temperature rise respectively).

Figure 18: Variation of temperature rise produced in a graphite wall by a train of exponentially-decaying heat flux pulses ($t_{1\%}$ is the time required for the surface heat flux to drop to 1% of its maximum value; $t_{1\%} = 4.61\ \tau$).

Figure 19: Variation of surface evaporation rate produced by different X-ray spectra during a pulse for a carbon wall with no gas protection.

Figure 20: Variation of amount of material evaporated during a pulse for a carbon wall with no gas protection (Ω = 0.01, 0.02, 0.05 correspond to a wall thickness of 6.5, 4.5, and 2.9 mm respectively).

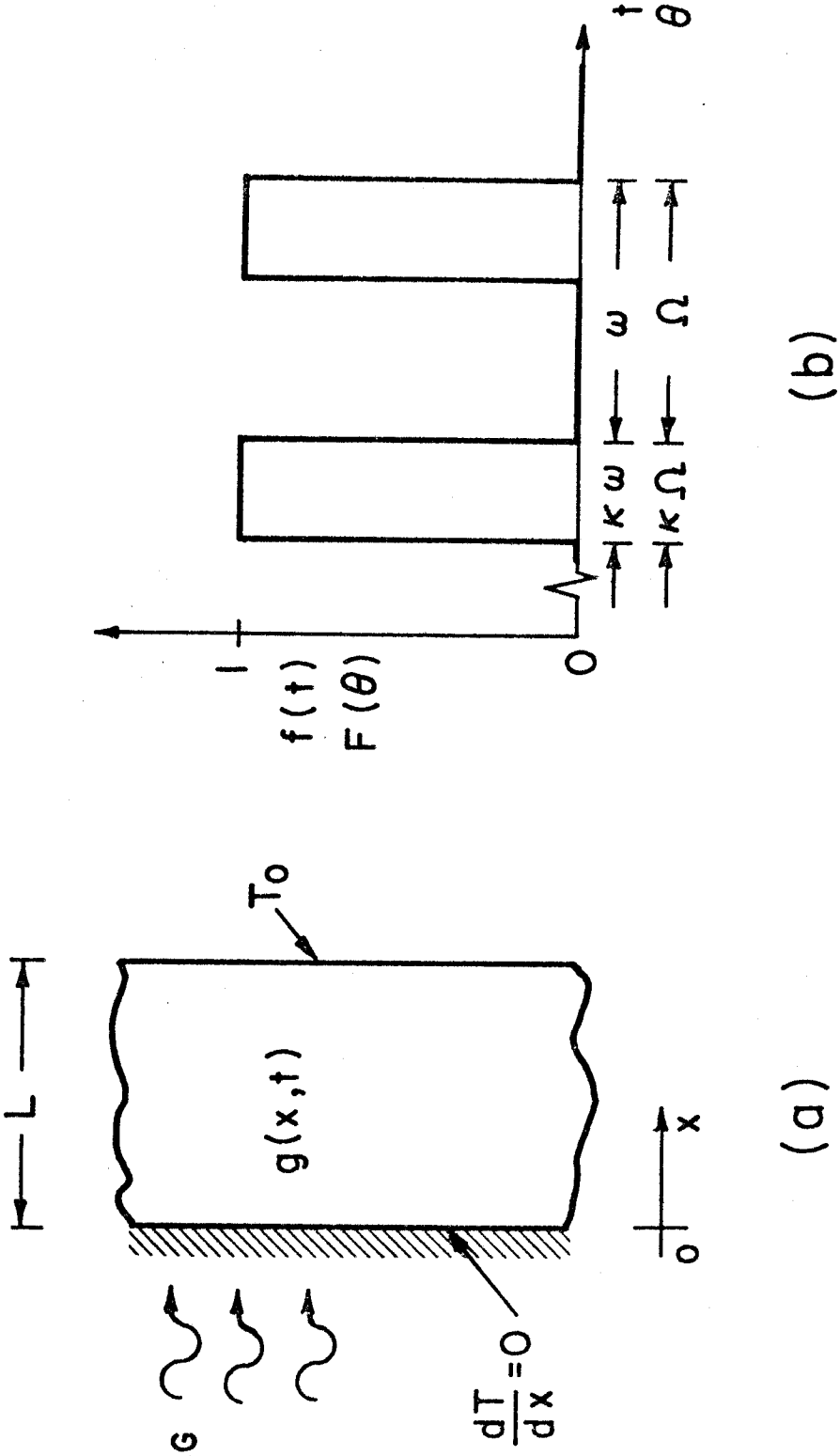
t
θ
ω
Ω
κω
κΩ
1
f(t)
F(θ)
0
(b)
T₀
L
g(x,t)
x
0
(a)
PULSATING
PHOTON
SOURCE
dT/dx=0

Figure 1

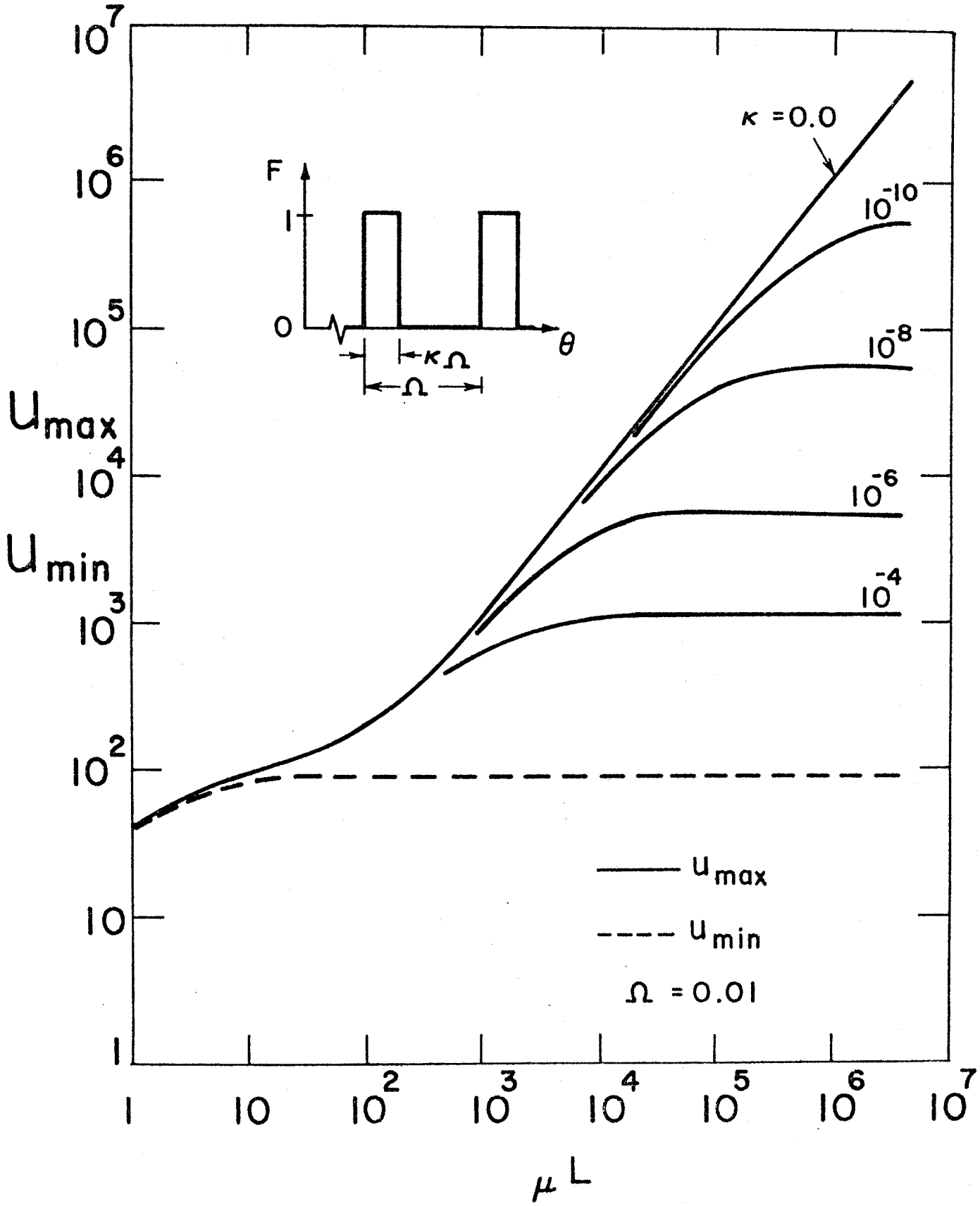
10^7
10^6
10^5
U_{max}
10^4
U_{min}
10^3
10^2
10
1
F
1
0
θ
κΩ
Ω
κ = 0.0
10^{-10}
10^{-8}
10^{-6}
10^{-4}
u_{max}
u_{min}
Ω = 0.01
1
10
10^2
10^3
10^4
10^5
10^6
10^7
μL

Figure 2

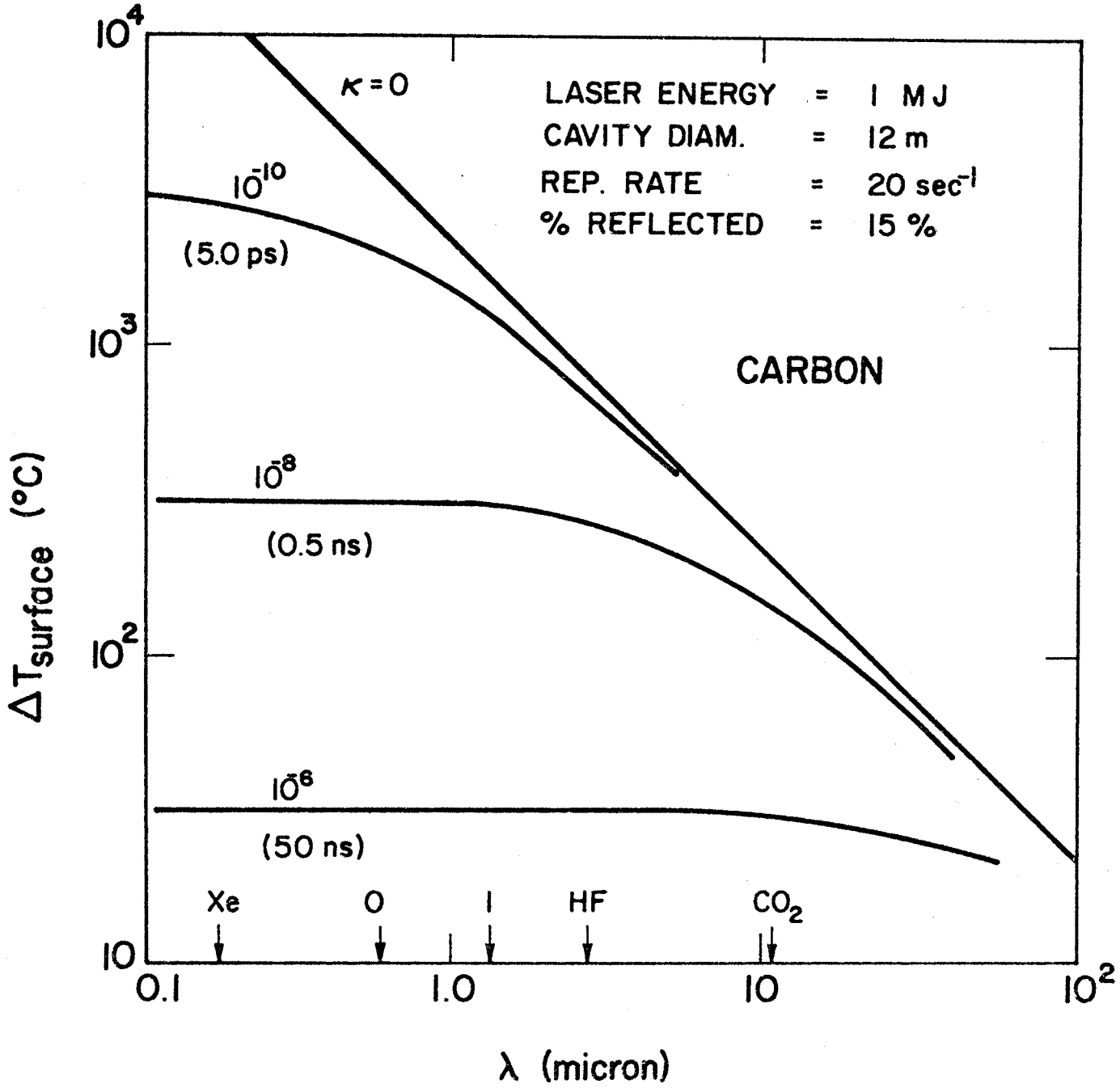
10^4
10^3
10^2
10
$\kappa = 0$
LASER ENERGY = 1 MJ
CAVITY DIAM. = 12 m
REP. RATE = 20 sec^{-1}
% REFLECTED = 15 %
10^{-10}
(5.0 ps)
CARBON
10^{-8}
(0.5 ns)
10^{-6}
(50 ns)
Xe
O
I
HF
CO_2
0.1
1.0
10
10^2
$\Delta T_{surface}$ (°C)
λ (micron)

Figure 3

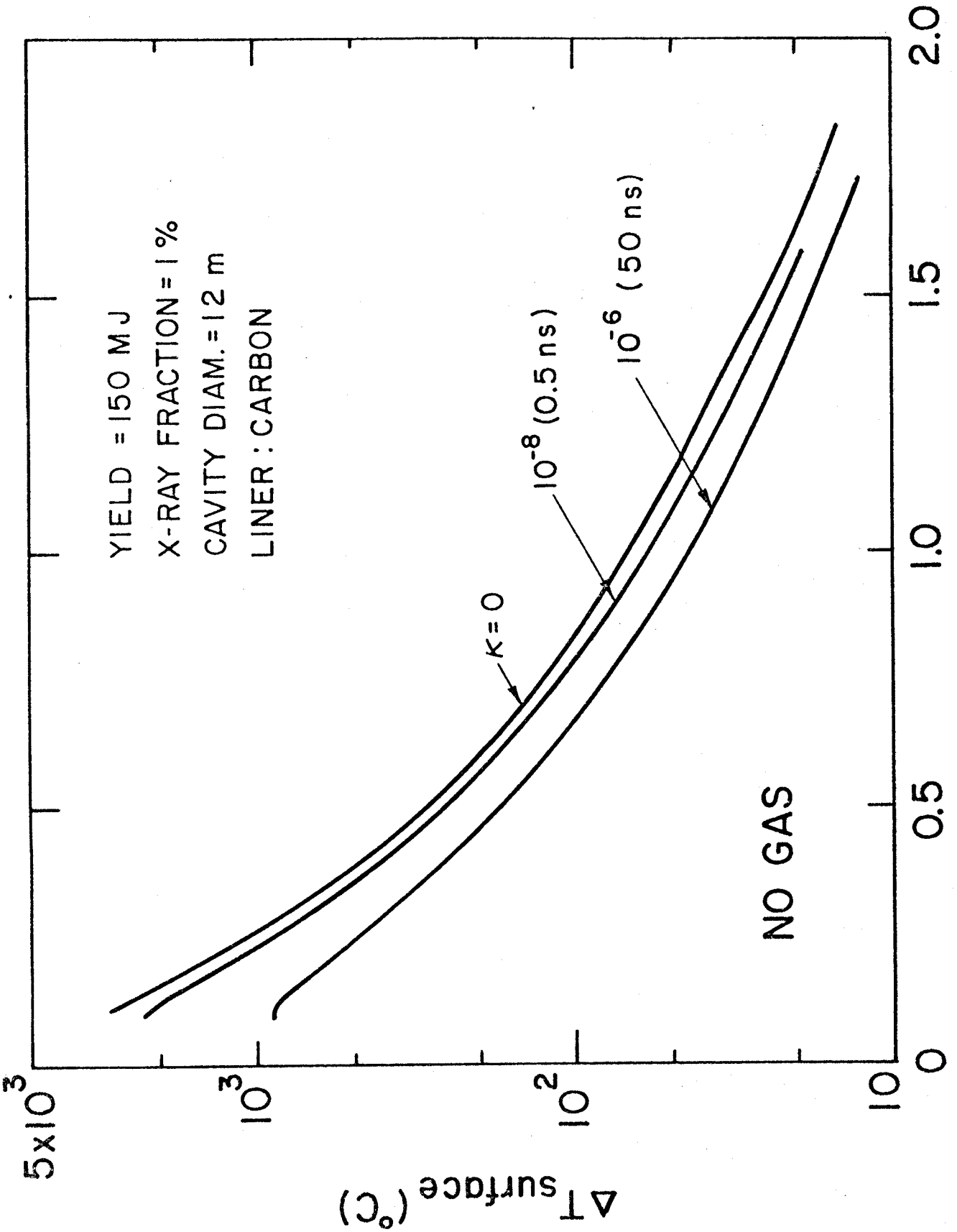
YIELD = 150 MJ
X-RAY FRACTION = 1 %
CAVITY DIAM. = 12 m
LINER : CARBON
10^{-8} (0.5 ns)
10^{-6} (50 ns)
K = 0
NO GAS
$\Delta T_{surface}$ (°C)
5×10^3
10^3
10^2
10
0
0.5
1.0
1.5
2.0
BLACKBODY TEMPERATURE (keV)

Figure 4

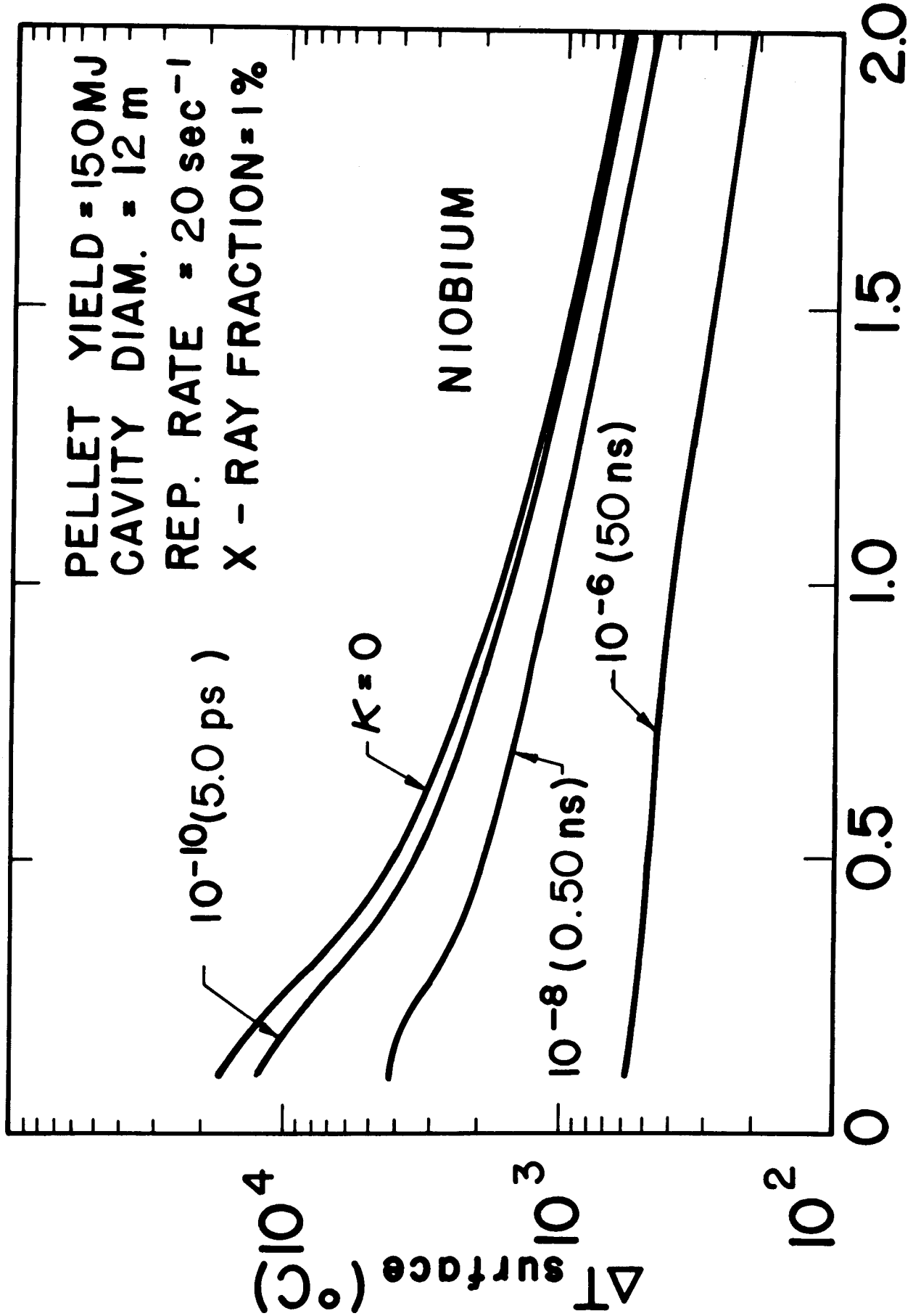
PELLET YIELD = 150MJ
CAVITY DIAM. = 12 m
REP. RATE = 20 sec⁻¹
X - RAY FRACTION = 1%
NIOBIUM
10⁻¹⁰(5.0 ps)
K = 0
10⁻⁸ (0.50 ns)
10⁻⁶ (50 ns)
ΔT surface (°C)
10⁴
10³
10²
0
0.5
1.0
1.5
2.0
BLACK BODY TEMP. (keV)

Figure 5

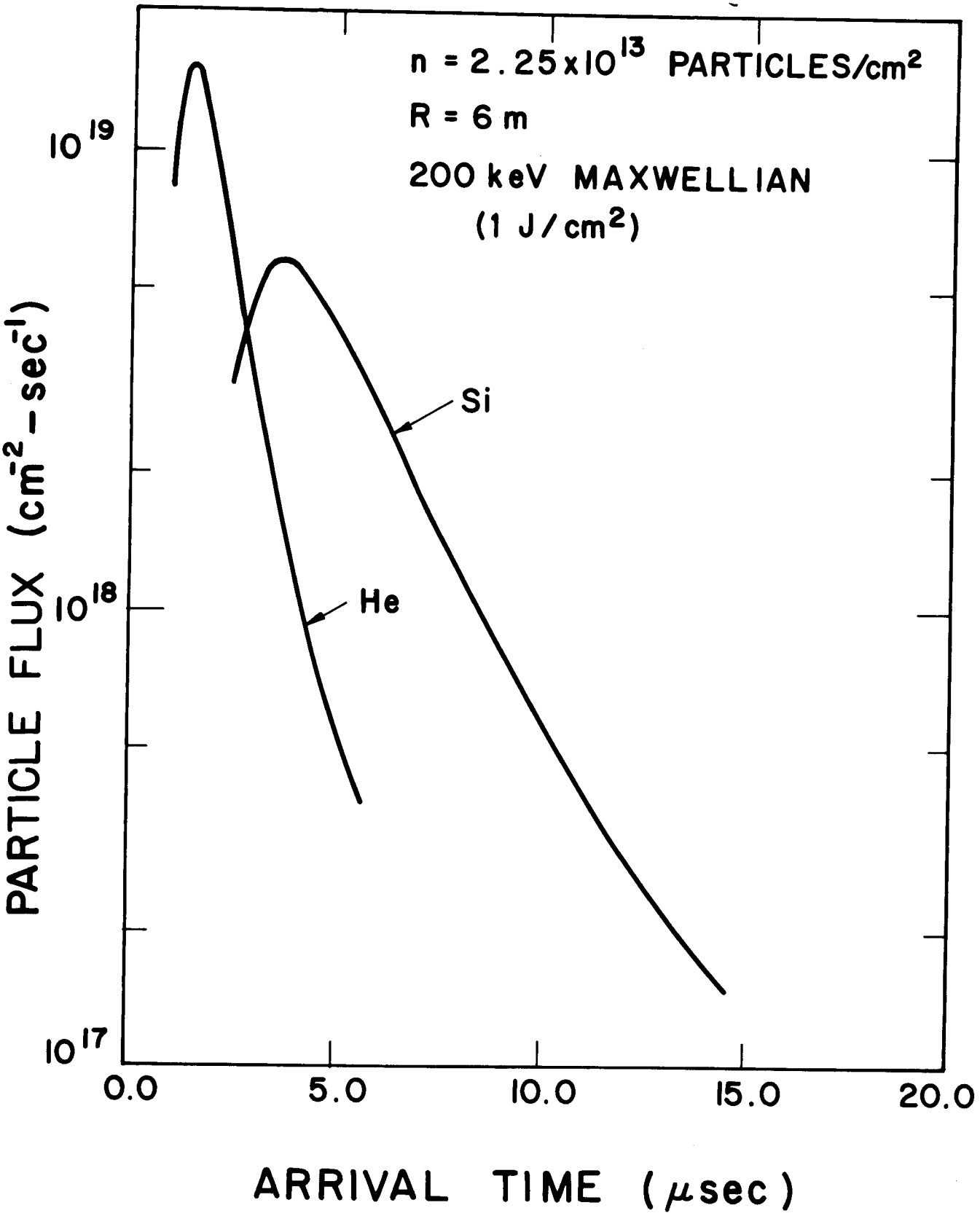
n = 2.25x10^13 PARTICLES/cm^2
R = 6 m
200 keV MAXWELLIAN
(1 J/cm^2)
Si
He
PARTICLE FLUX (cm^-2-sec^-1)
10^19
10^18
10^17
0.0
5.0
10.0
15.0
20.0
ARRIVAL TIME (μsec)

Figure 6

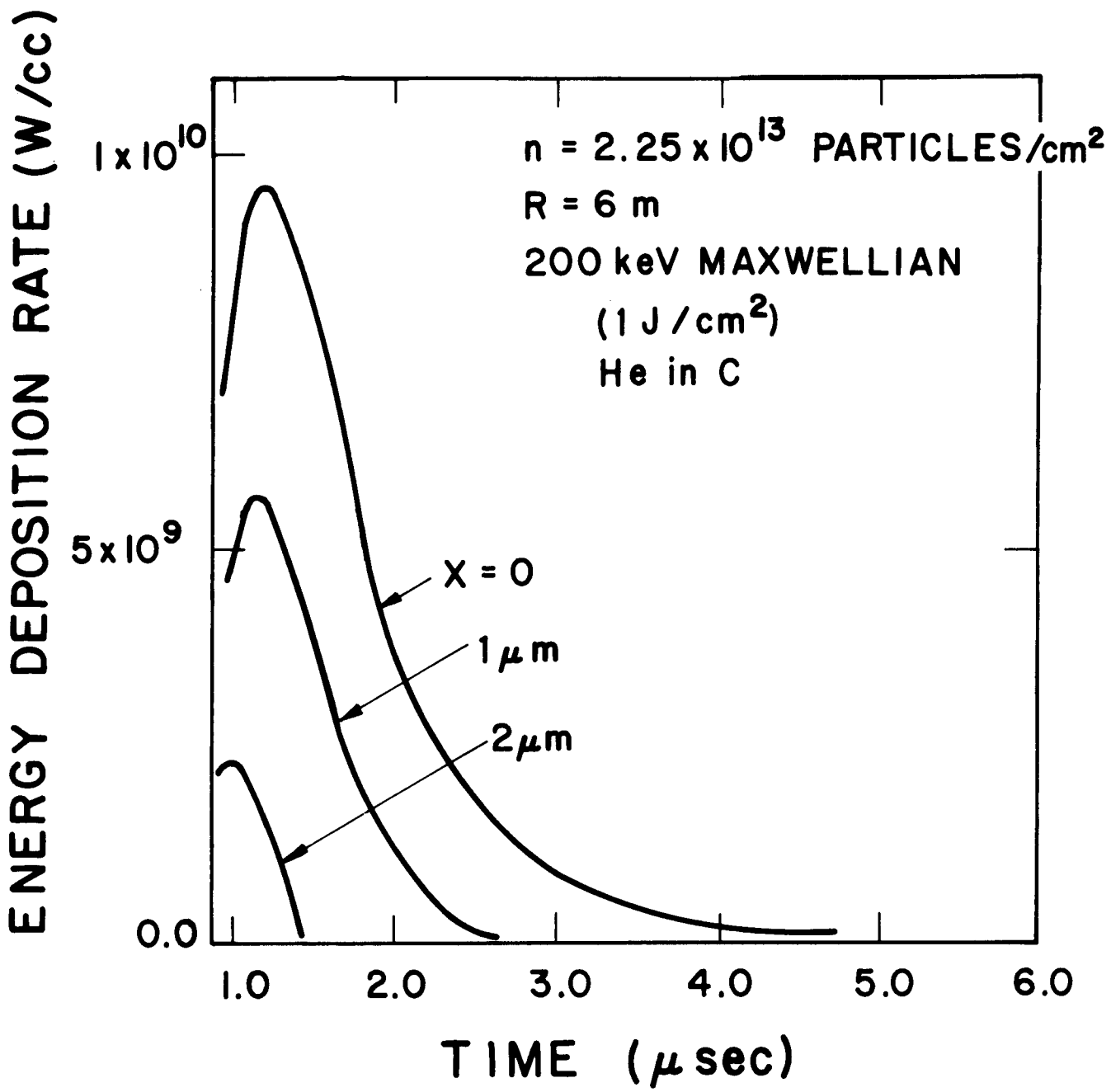
ENERGY DEPOSITION RATE (W/cc)
1 x 10^10
5 x 10^9
0.0
n = 2.25 x 10^13 PARTICLES/cm^2
R = 6 m
200 keV MAXWELLIAN
(1 J/cm^2)
He in C
X = 0
1 μm
2 μm
1.0
2.0
3.0
4.0
5.0
6.0
TIME (μsec)

Figure 7

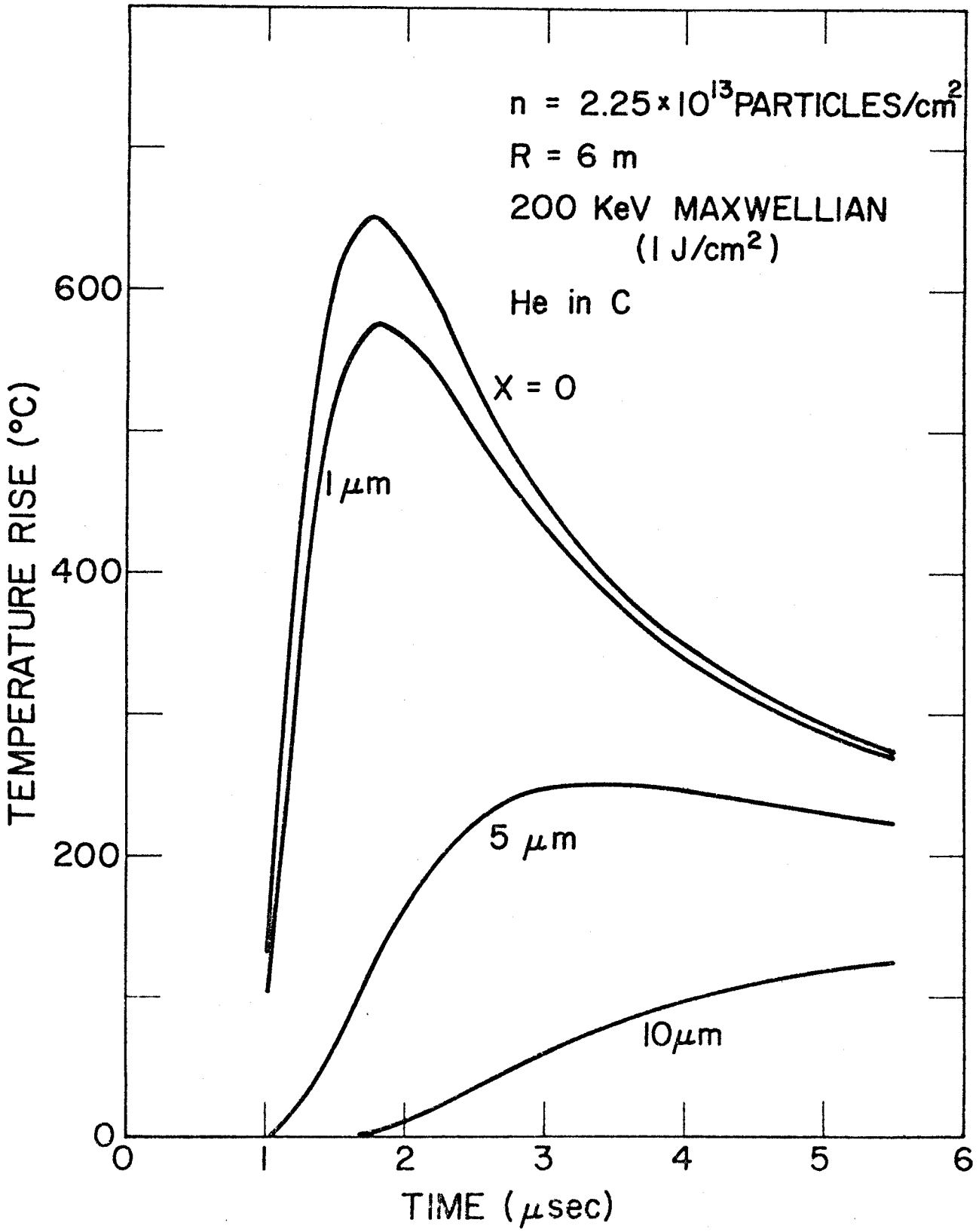
n = 2.25 × 10^13 PARTICLES/cm^2
R = 6 m
200 KeV MAXWELLIAN
(1 J/cm^2)
He in C
X = 0
1 μm
5 μm
10μm
TEMPERATURE RISE (°C)
600
400
200
0
0
1
2
3
4
5
6
TIME (μsec)

Figure 8

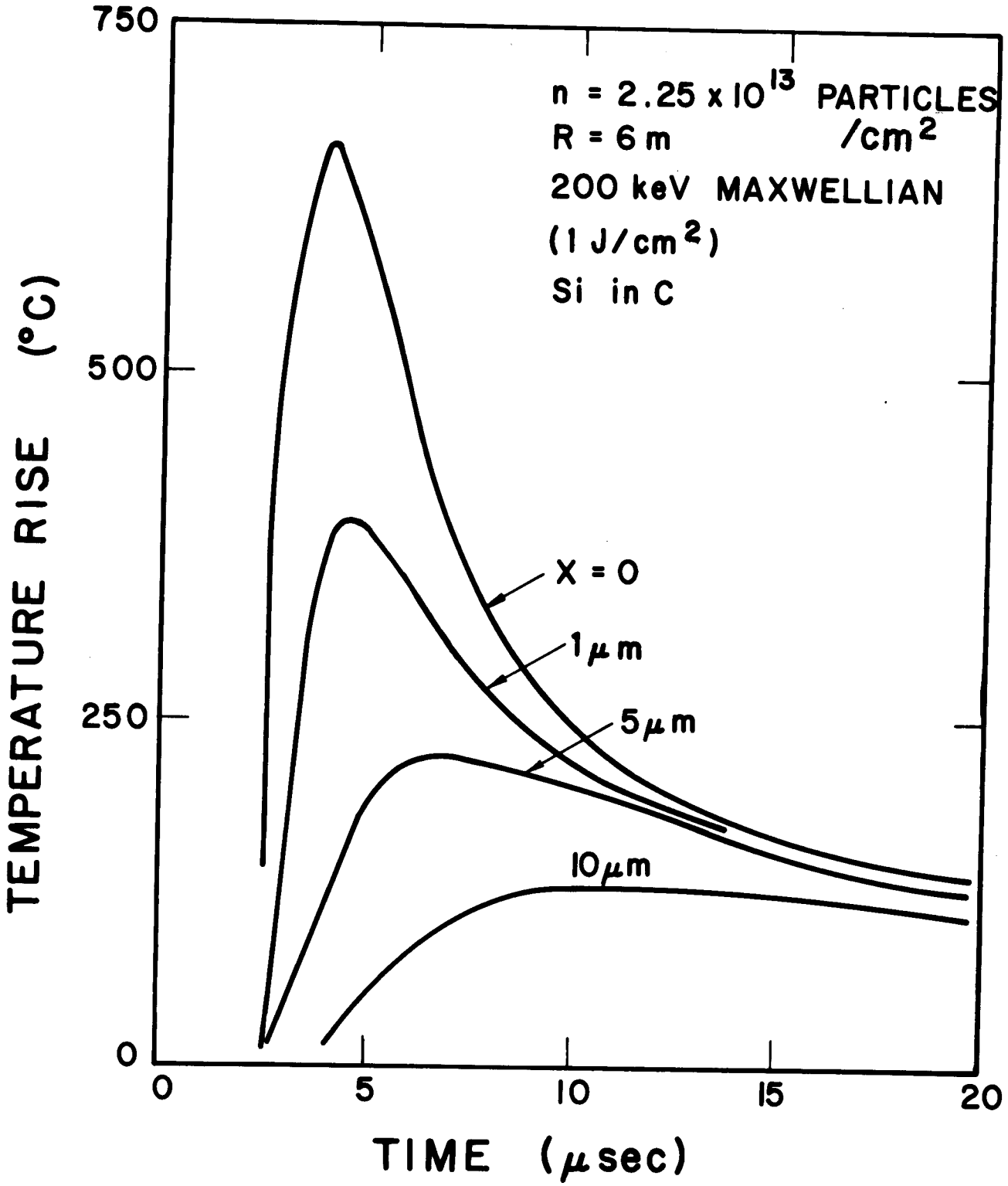
750
500
250
0
0
5
10
15
20
TEMPERATURE RISE (°C)
TIME (μsec)
n = 2.25 x 10^13 PARTICLES /cm^2
R = 6 m
200 keV MAXWELLIAN
(1 J/cm^2)
Si in C
X = 0
1μm
5μm
10μm

Figure 9

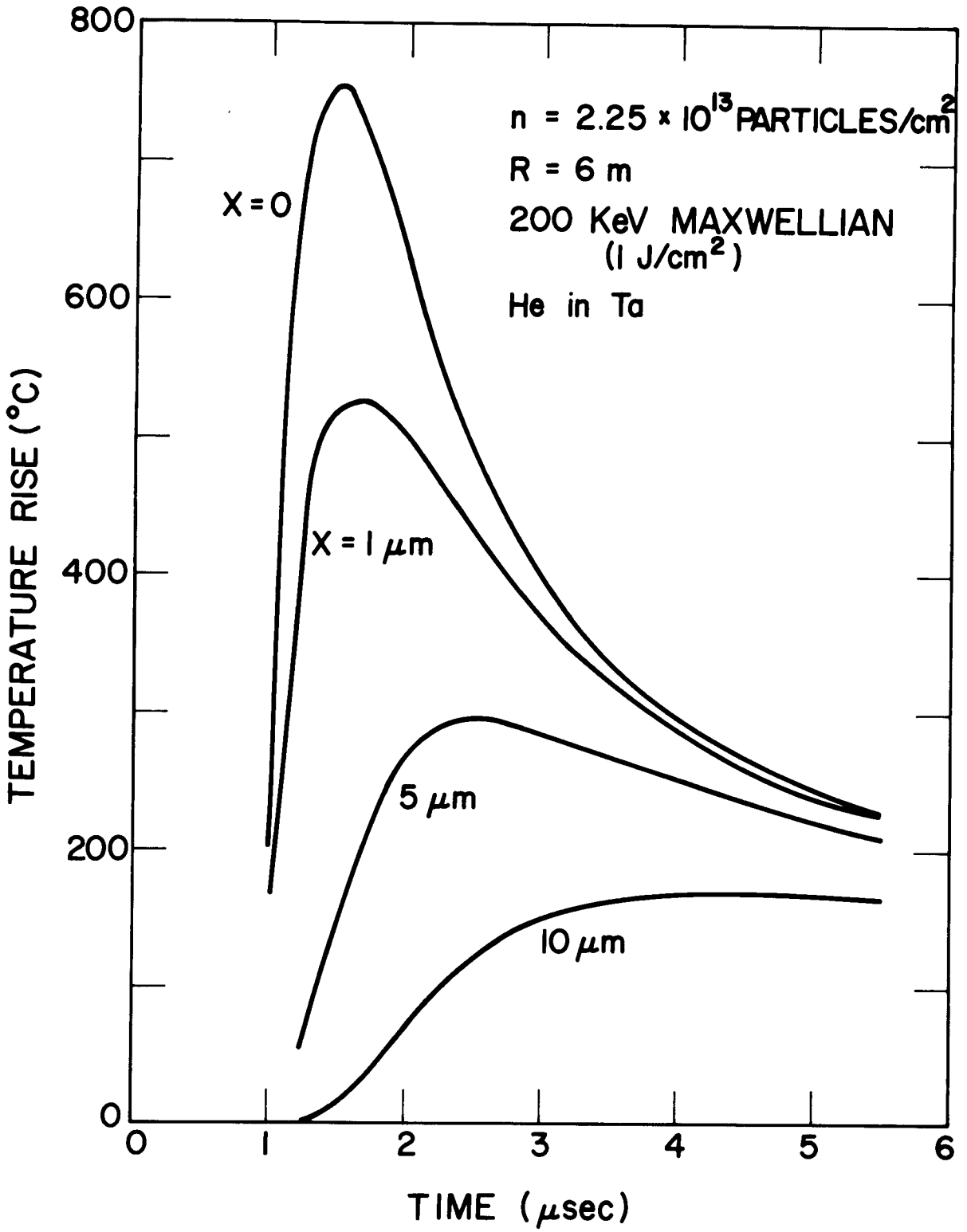
800
600
400
200
0
0
1
2
3
4
5
6
TEMPERATURE RISE (°C)
TIME (μsec)
n = 2.25 × 10^13 PARTICLES/cm^2
R = 6 m
200 KeV MAXWELLIAN
(1 J/cm^2)
He in Ta
X = 0
X = 1 μm
5 μm
10 μm

Figure 10

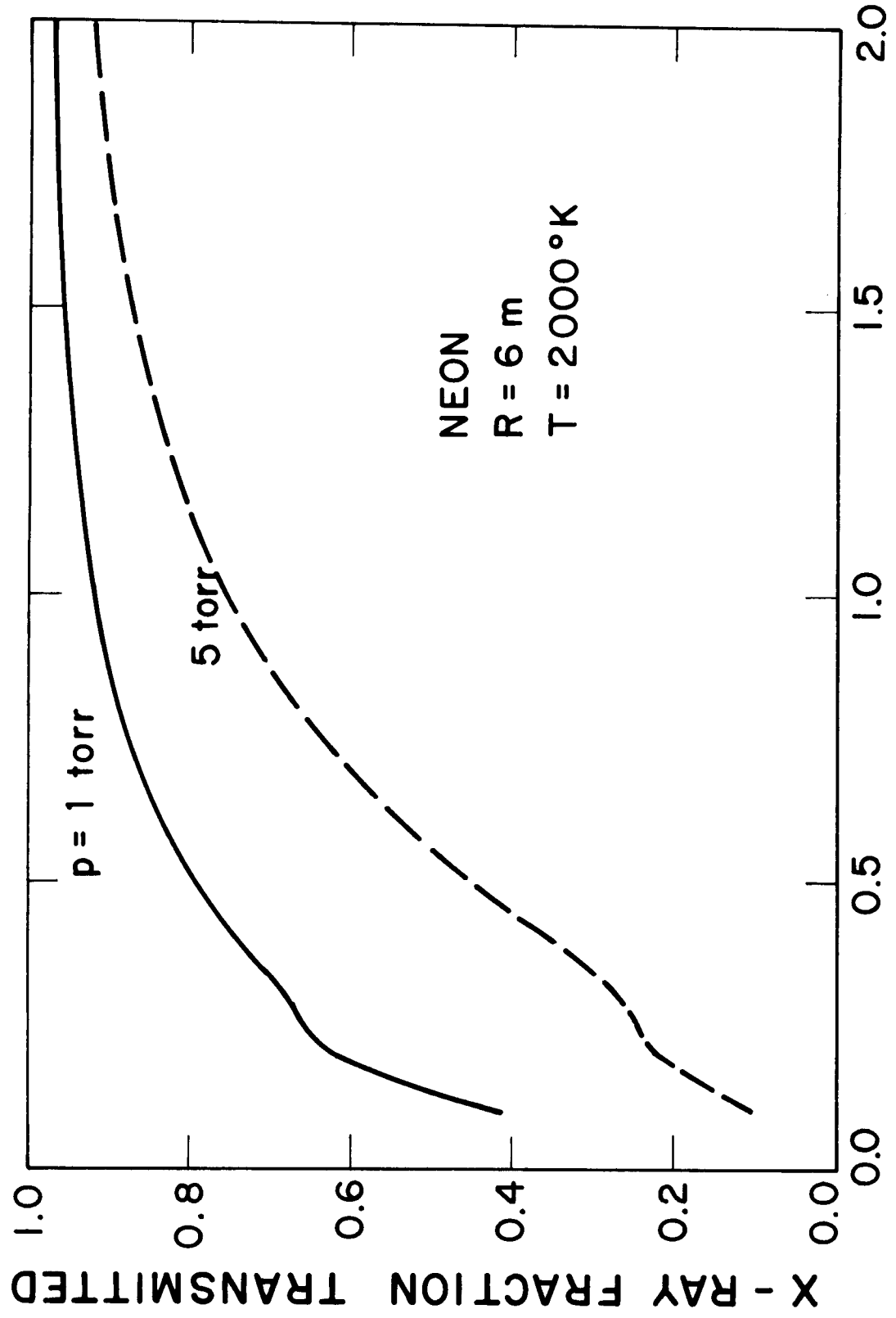
X - RAY FRACTION TRANSMITTED
1.0
0.8
0.6
0.4
0.2
0.0
0.0
0.5
1.0
1.5
2.0
BLACKBODY TEMPERATURE (keV)
NEON
R = 6 m
T = 2000°K
p = 1 torr
5 torr

Figure 11

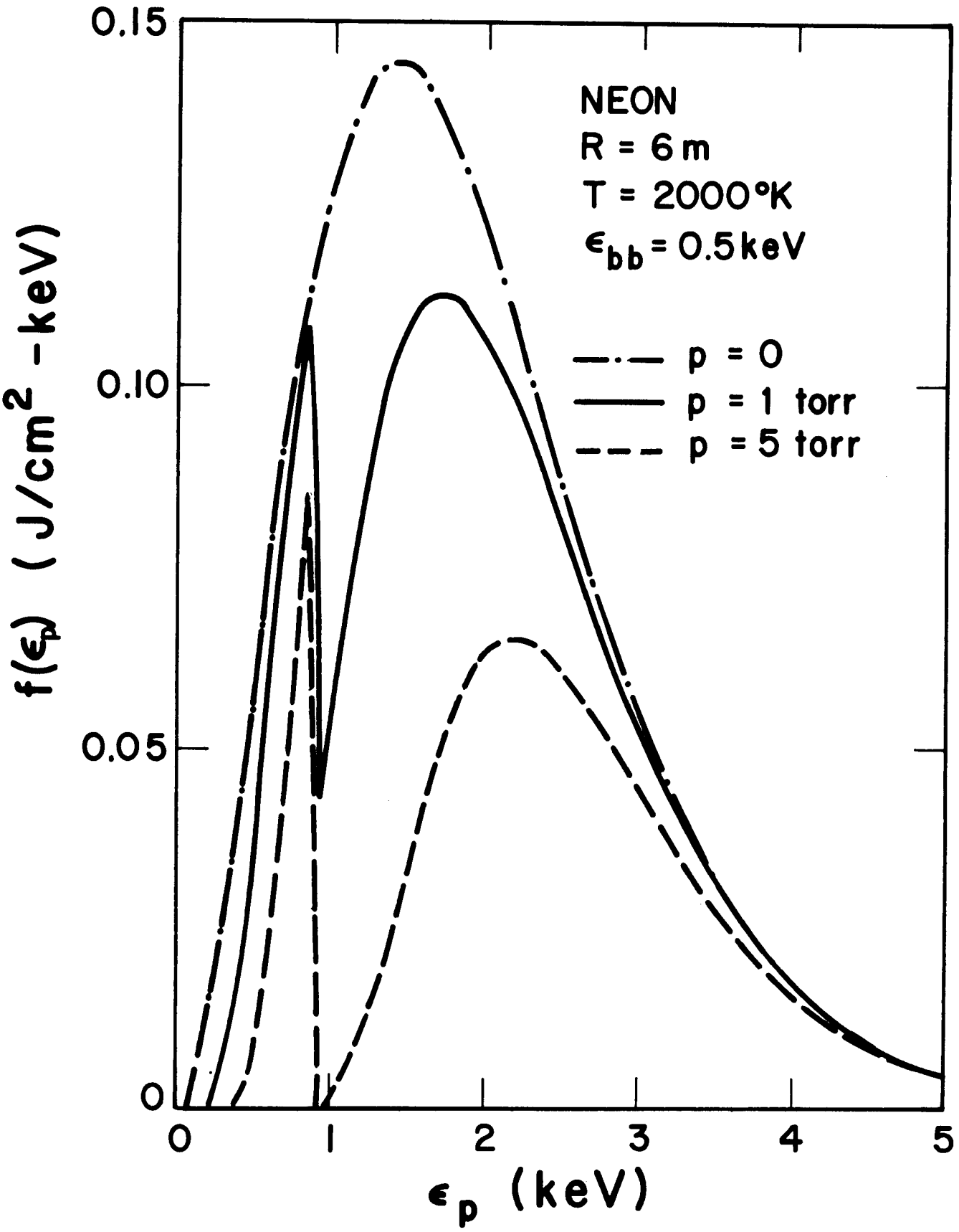
NEON
R = 6 m
T = 2000°K
ϵ_{bb} = 0.5keV
p = 0
p = 1 torr
p = 5 torr
f(ϵ_p) (J/cm^2-keV)
0.15
0.10
0.05
0
0
1
2
3
4
5
ϵ_p (keV)

Figure 12

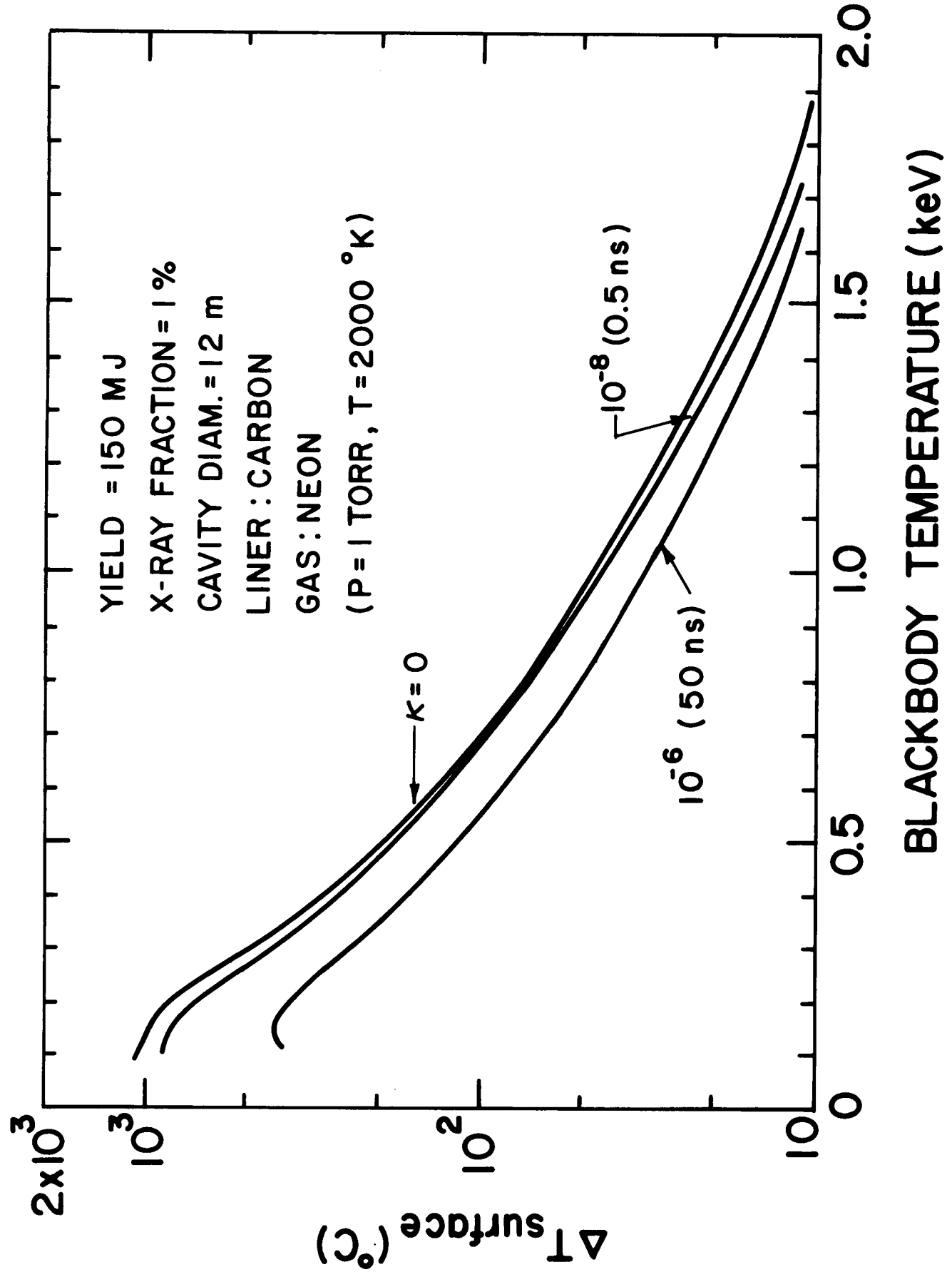
YIELD = 150 MJ
X-RAY FRACTION = 1 %
CAVITY DIAM. = 12 m
LINER : CARBON
GAS : NEON
(P = 1 TORR, T = 2000 °K)
κ = 0
10^-8 (0.5 ns)
10^-6 (50 ns)
ΔT surface (°C)
2x10^3
10^3
10^2
10
0
0.5
1.0
1.5
2.0
BLACKBODY TEMPERATURE (keV)

Figure 13

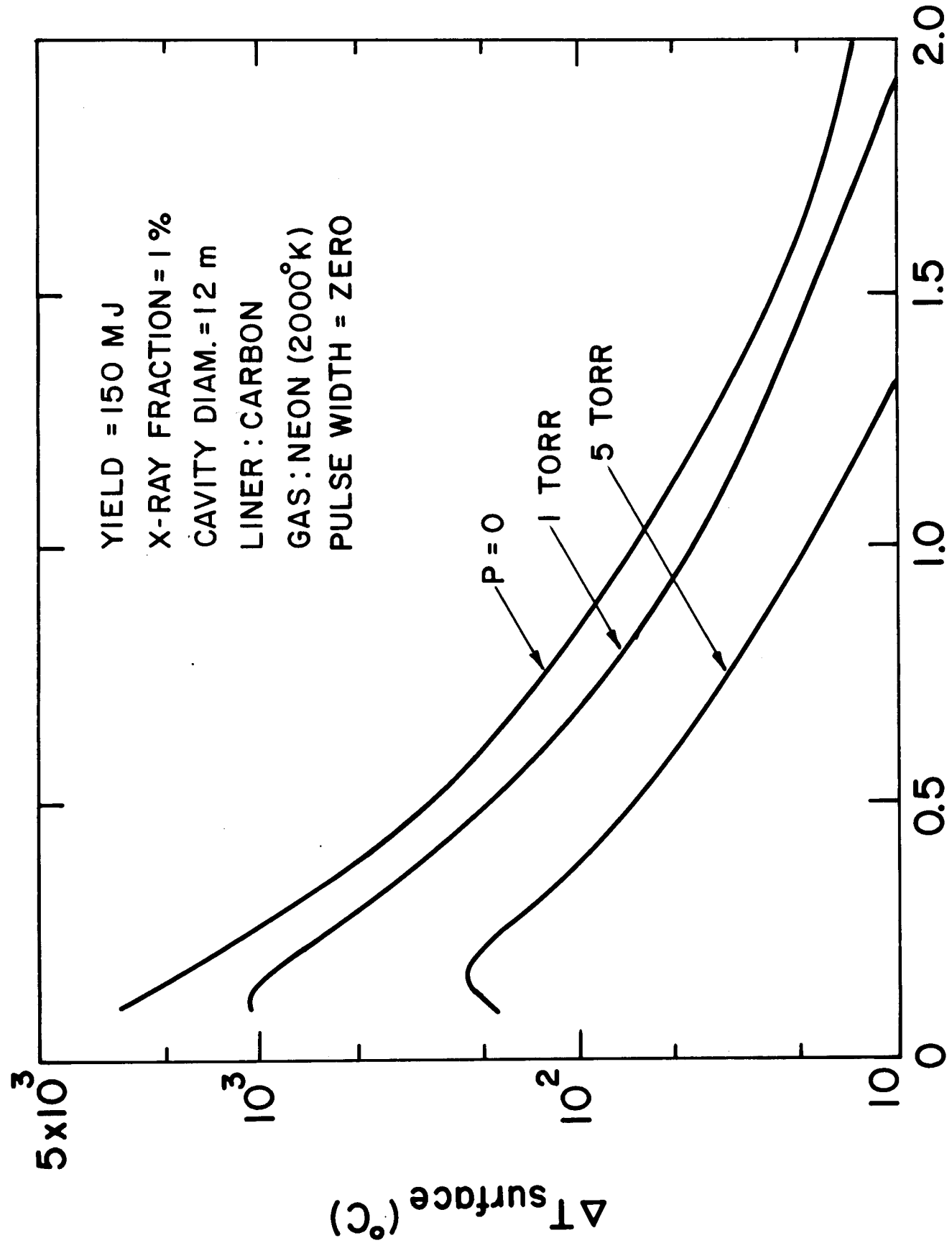
YIELD = 150 MJ
X-RAY FRACTION = 1 %
CAVITY DIAM. = 12 m
LINER : CARBON
GAS : NEON (2000°K)
PULSE WIDTH = ZERO
P = 0
1 TORR
5 TORR
$\Delta T_{surface}$ (°C)
5×10^3
10^3
10^2
10
0
0.5
1.0
1.5
2.0
BLACKBODY TEMPERATURE (keV)

Figure 14

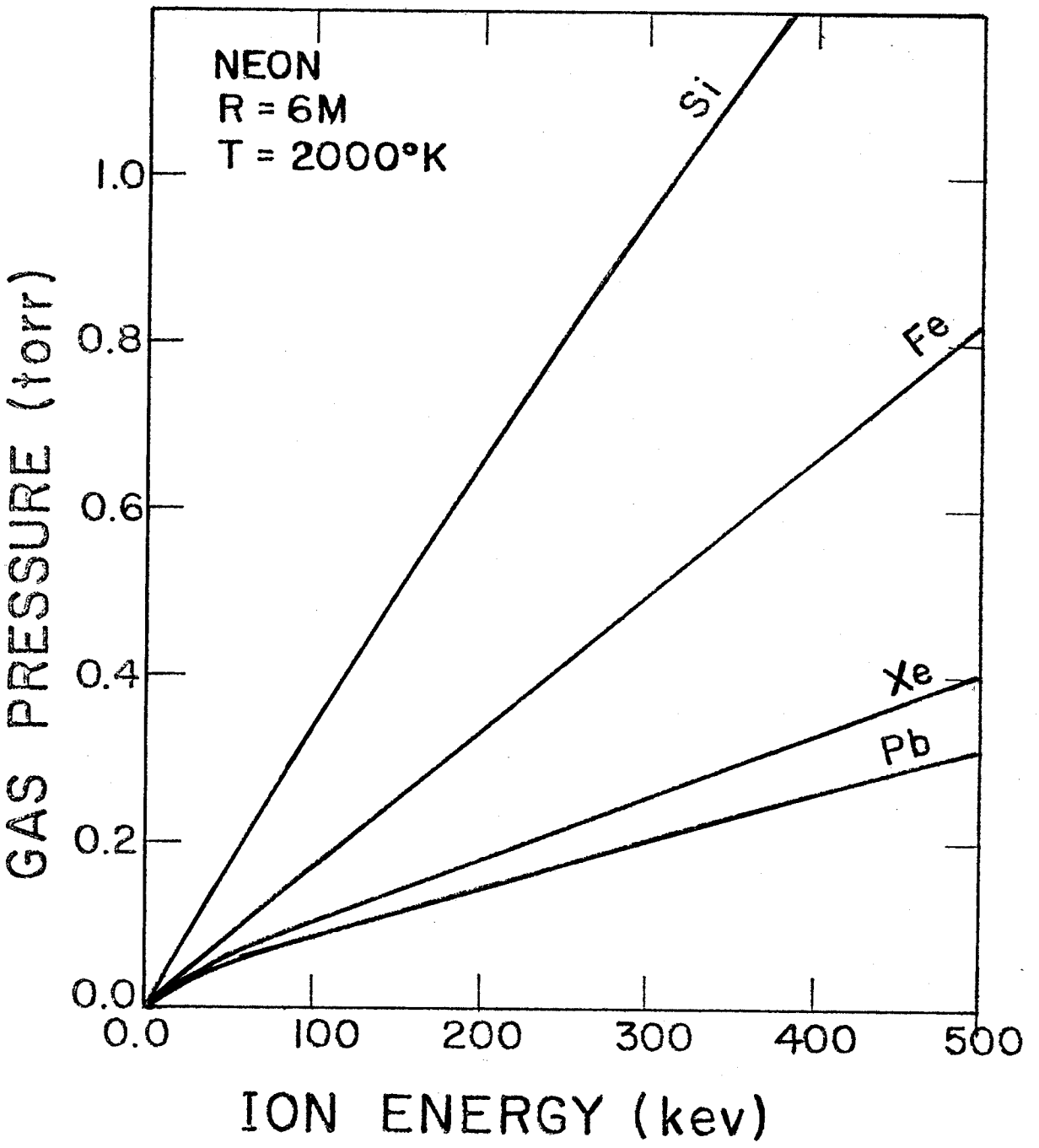
NEON
R = 6M
T = 2000°K
Si
Fe
Xe
Pb
GAS PRESSURE (torr)
1.0
0.8
0.6
0.4
0.2
0.0
0.0
100
200
300
400
500
ION ENERGY (kev)

Figure 15

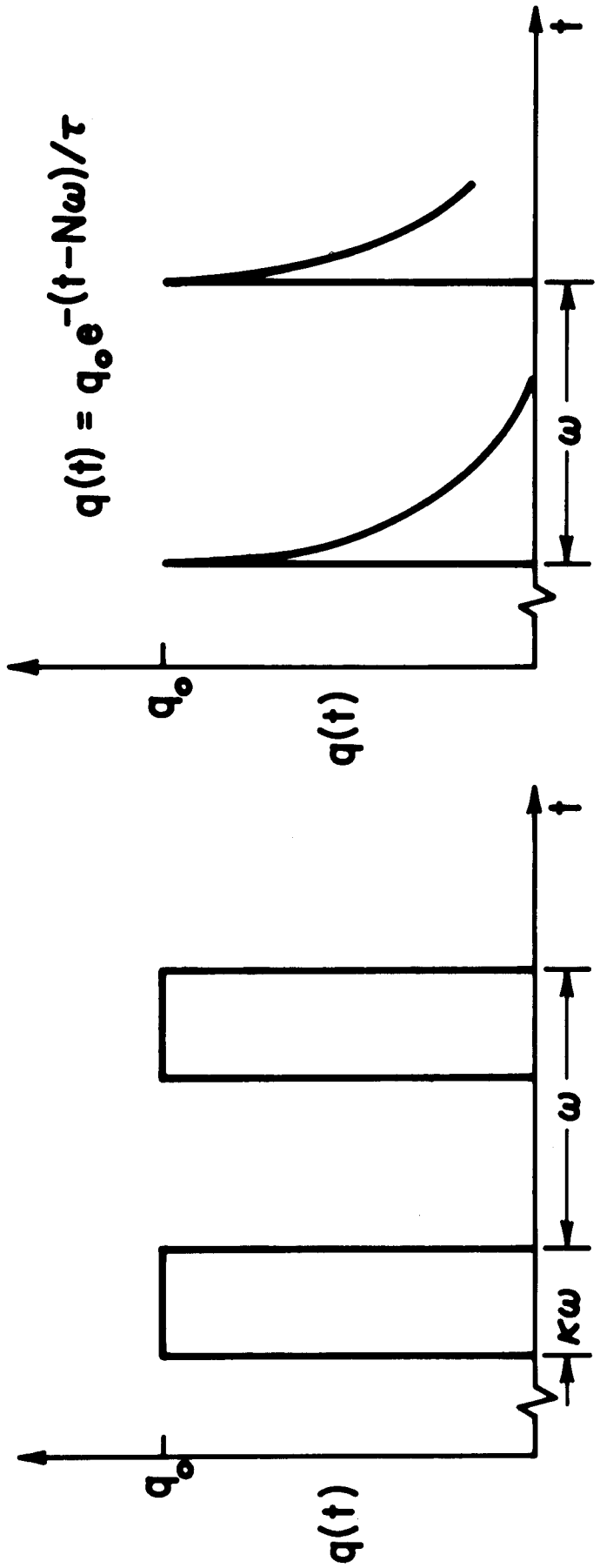

Figure 16

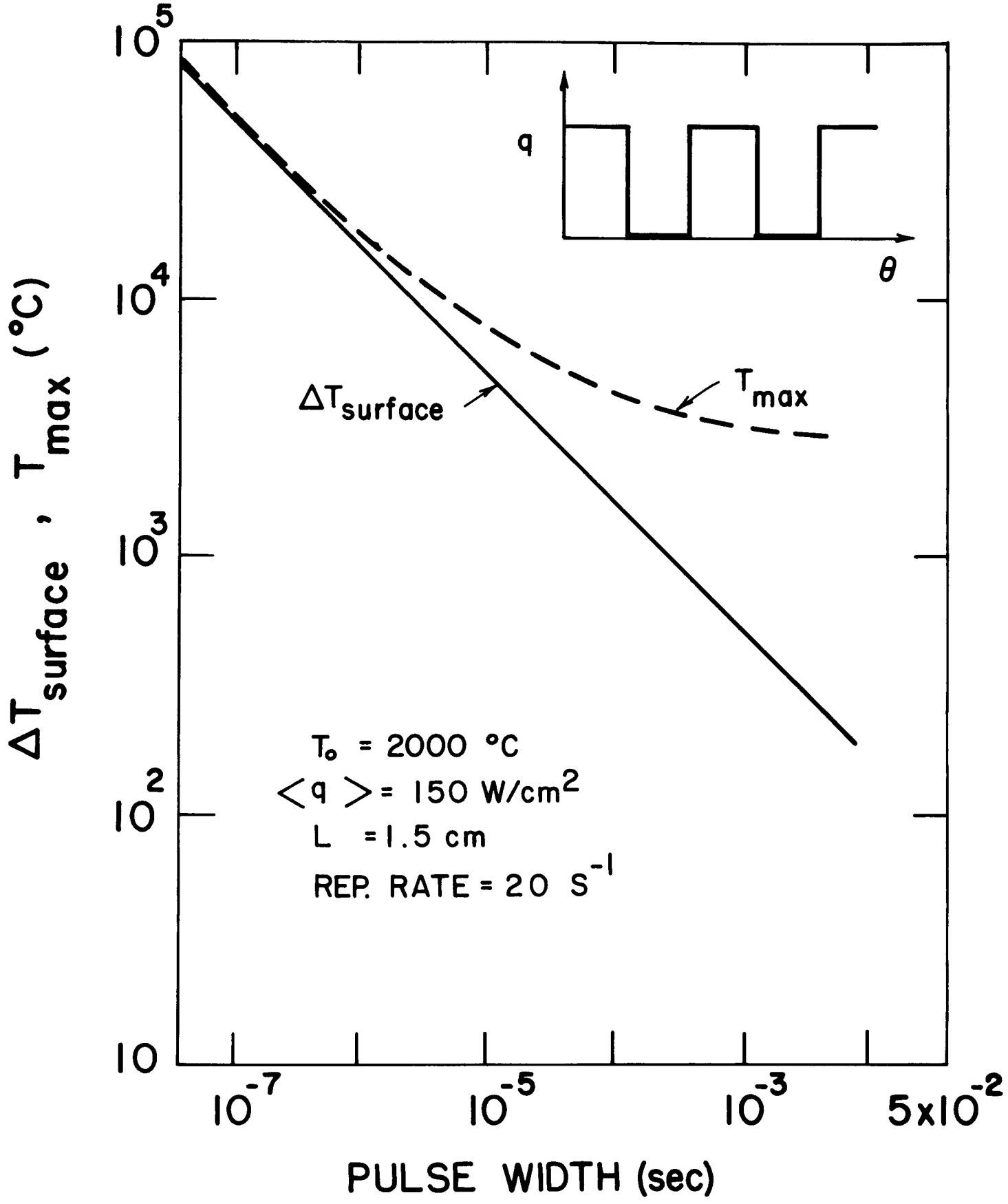
10^5
10^4
10^3
10^2
10
$\Delta T_{surface}$, T_{max} (°C)
q
θ
$\Delta T_{surface}$
T_{max}
T_o = 2000 °C
$\langle q \rangle$ = 150 W/cm^2
L = 1.5 cm
REP. RATE = 20 S^{-1}
10^{-7}
10^{-5}
10^{-3}
5×10^{-2}
PULSE WIDTH (sec)

Figure 17

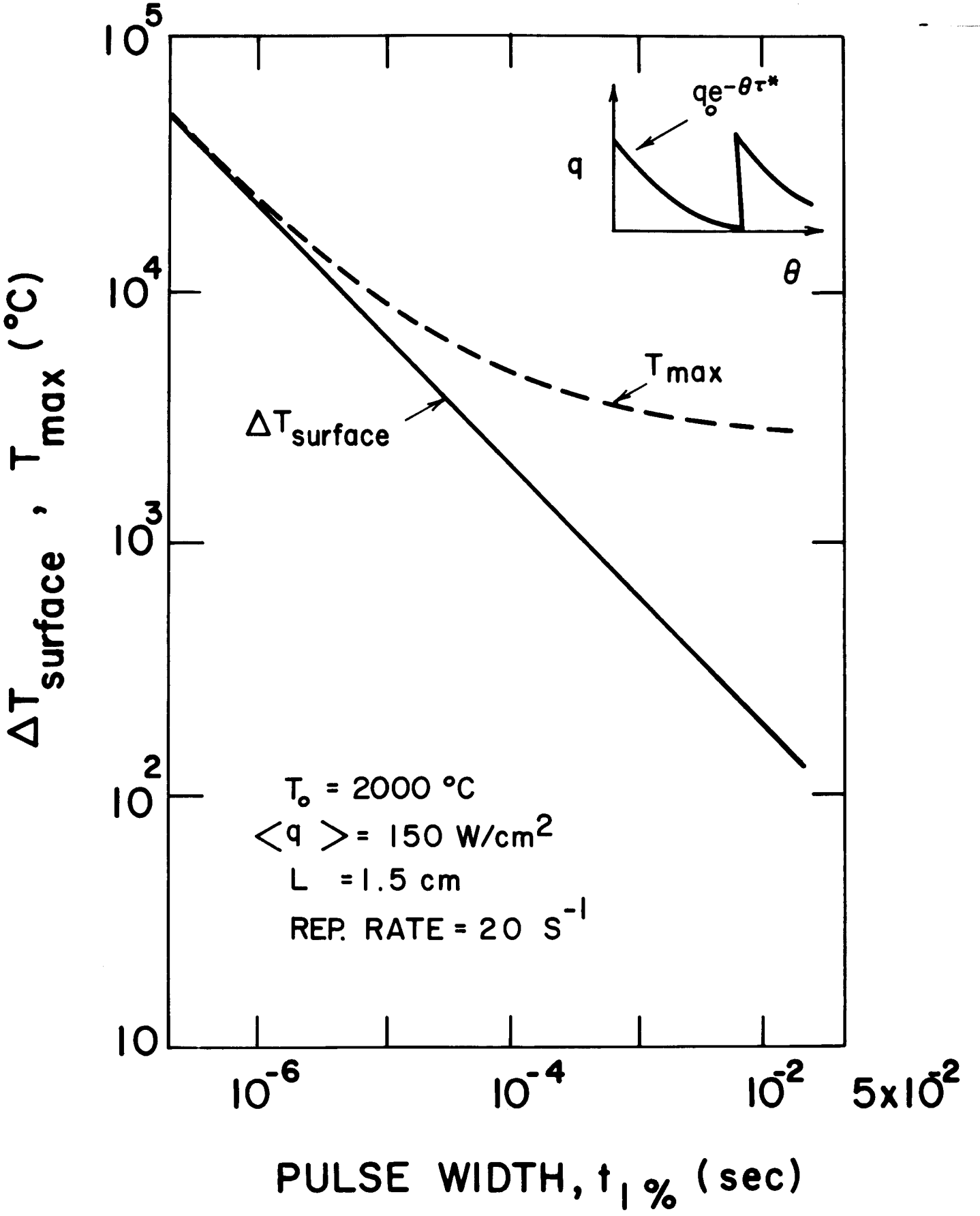
10^5
10^4
10^3
10^2
10
$\Delta T_{surface}$, T_{max} (°C)
$qe^{-\theta\tau^*}$
q
θ
T_{max}
$\Delta T_{surface}$
T_o = 2000 °C
<q> = 150 W/cm²
L = 1.5 cm
REP. RATE = 20 s^{-1}
10^{-6}
10^{-4}
10^{-2}
$5x10^{-2}$
PULSE WIDTH, $t_{1\%}$ (sec)

Figure 18

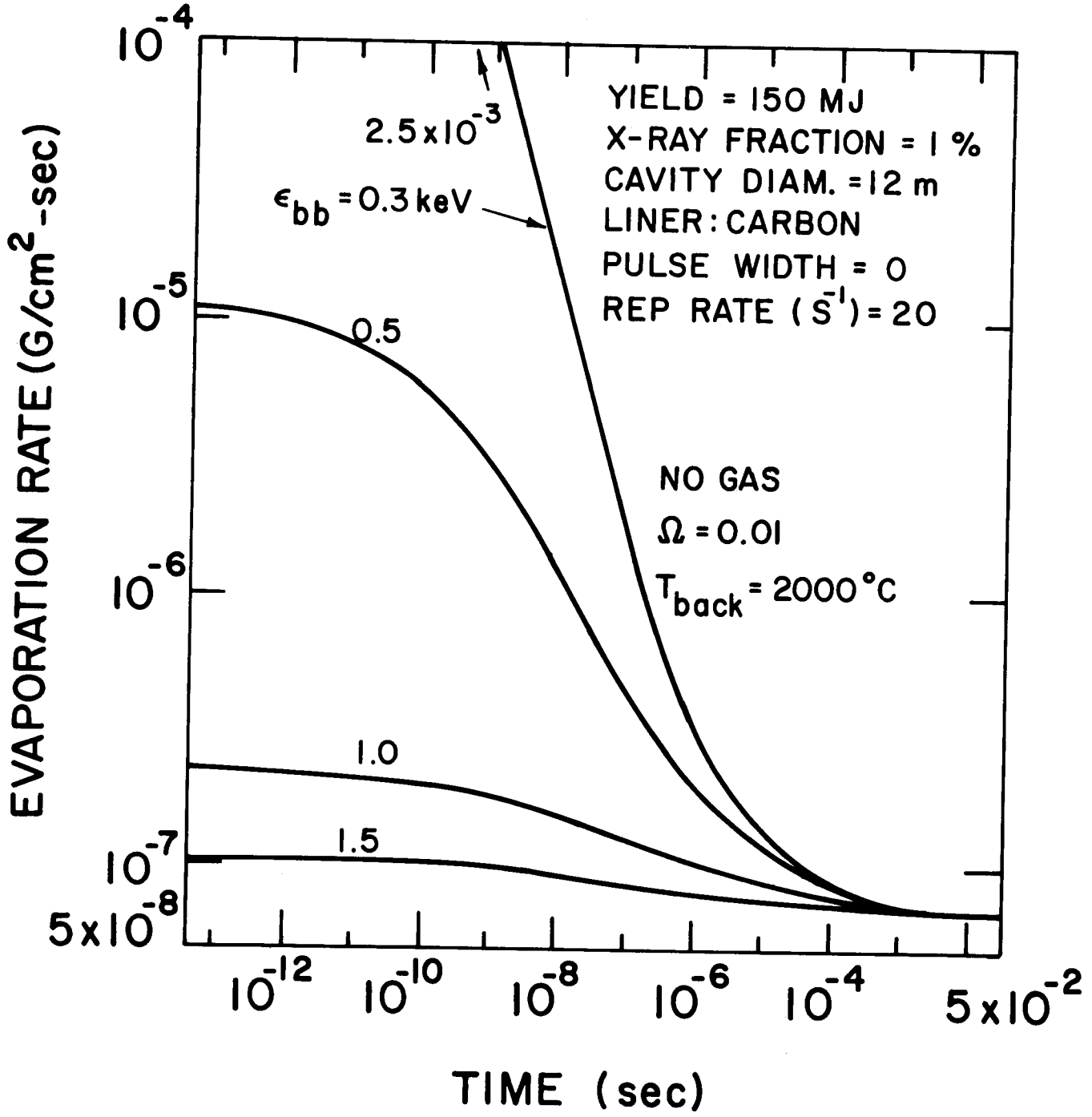
EVAPORATION RATE (G/cm²-sec)
TIME (sec)
YIELD = 150 MJ
X-RAY FRACTION = 1 %
CAVITY DIAM. = 12 m
LINER: CARBON
PULSE WIDTH = 0
REP RATE (S⁻¹) = 20
NO GAS
Ω = 0.01
T_back = 2000°C
2.5x10⁻³
ε_bb = 0.3 keV
0.5
1.0
1.5
10⁻⁴
10⁻⁵
10⁻⁶
10⁻⁷
5x10⁻⁸
10⁻¹²
10⁻¹⁰
10⁻⁸
10⁻⁶
10⁻⁴
5x10⁻²

Figure 19

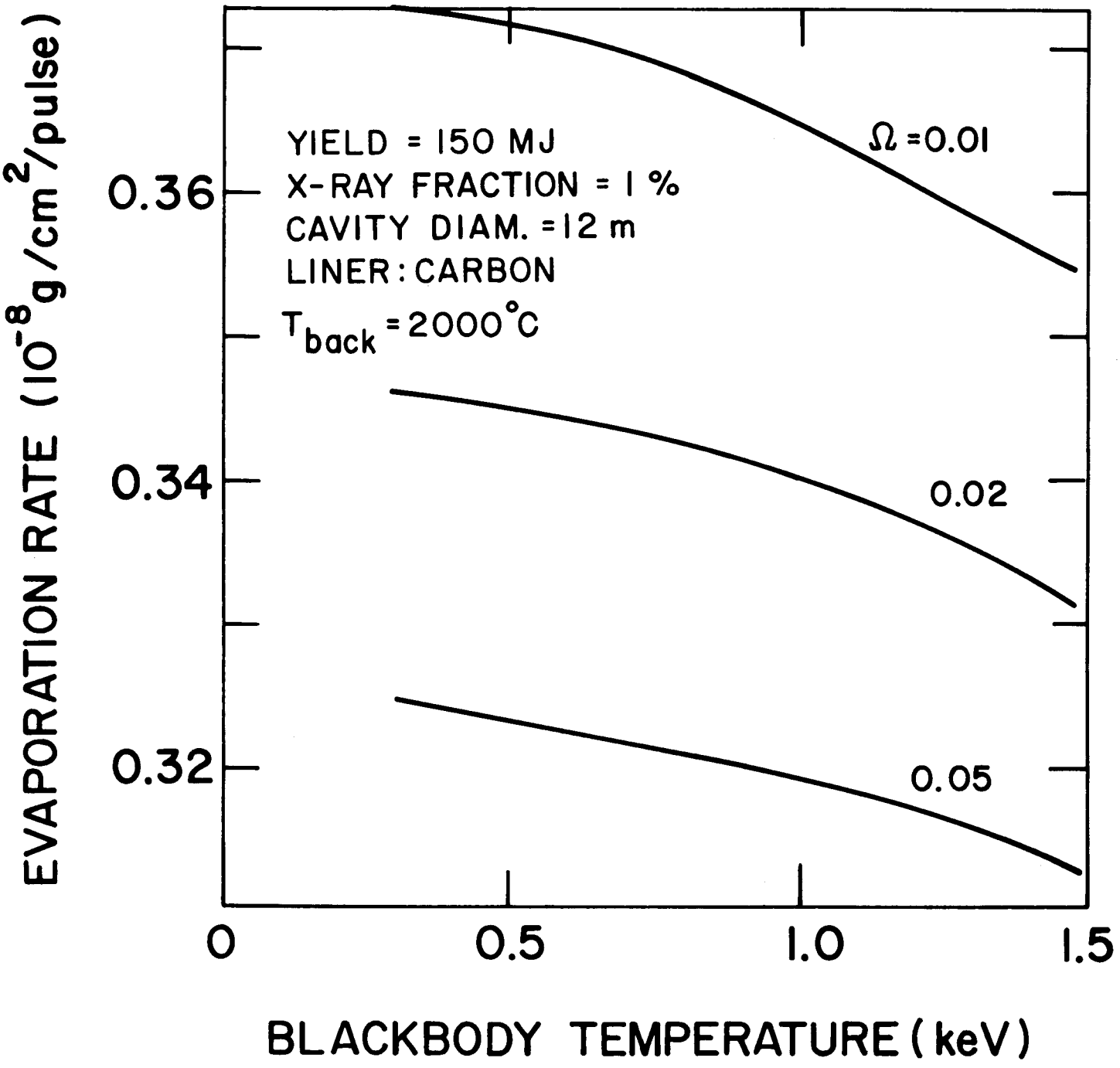
EVAPORATION RATE (10^{-8} g/cm^2/pulse)
0.36
0.34
0.32
YIELD = 150 MJ
X-RAY FRACTION = 1 %
CAVITY DIAM. = 12 m
LINER: CARBON
T_{back} = 2000°C
Ω = 0.01
0.02
0.05
0
0.5
1.0
1.5
BLACKBODY TEMPERATURE (keV)

Figure 20